

GENERATIVE MODELING WITH PHASE STOCHASTIC BRIDGES

Tianrong Chen^{1*}, Jiatao Gu², Laurent Dinh²,

Evangelos A. Theodorou¹, Josh Susskind², Shuangfei Zhai²

¹Georgia Tech, ²Apple

{tianrong.chen, evangelos.theodorou}@gatech.edu, {jgu32,1_dinh,jsusskind,szhai}@apple.com

ABSTRACT

Diffusion models (DMs) represent state-of-the-art generative models for continuous inputs. DMs work by constructing a Stochastic Differential Equation (SDE) in the input space (ie, position space), and using a neural network to reverse it. In this work, we introduce a novel generative modeling framework grounded in **phase space dynamics**, where a phase space is defined as an augmented space encompassing both position and velocity. Leveraging insights from Stochastic Optimal Control, we construct a path measure in the phase space that enables efficient sampling. In contrast to DMs, our framework demonstrates the capability to generate realistic data points at an early stage of dynamics propagation. This early prediction sets the stage for efficient data generation by leveraging additional velocity information along the trajectory. On standard image generation benchmarks, our model yields favorable performance over baselines in the regime of small Number of Function Evaluations (NFEs). Furthermore, our approach rivals the performance of diffusion models equipped with efficient sampling techniques, underscoring its potential as a new tool generative modeling.

1 INTRODUCTION

Diffusion Models (DMs; Song et al. (2020a); Ho et al. (2020)) constitute an instrumental technique in generative modeling, which formulate a particular Stochastic Differential Equation (SDE) linking the data distribution with a tractable prior distribution. Initially, a DM diffuses data towards the prior distribution via a predetermined linear SDE. In order to reverse the process, a neural network is used to approximate the score function which is analytically available. Subsequently, the approximated score is utilized to conduct time reversal (Anderson, 1982; Haussmann & Pardoux, 1986) of this diffusion process, ultimately generating data. Recently, the Critical-damped Langevin Dynamics (CLD; Dockhorn et al. (2021)) extends the SDE framework of DM into phase space (whereas DMs operate in the position space) by introducing an auxiliary velocity variable, which is defined by tractable Gaussian distributions at the initial and terminal time steps. This augmentation induces a trajectory in position space exhibiting enhanced smoothness, as stochasticity is solely introduced into the velocity space. The distinctive structure of CLD is shown to enhance the empirical performance and sample efficiency. However, despite the success of CLD, inefficient sampling still persists due to unnecessary curvature of the dynamics (Fig.1) as it has to converge to equilibrium for sampling from the tractable prior.

The remarkable accomplishments of DM have also catalyzed recent advancements in generative modeling, leading to the development of Bridge Matching (BM; (Peluchetti, 2021; Liu et al., 2022; 2023)) and Flow Matching (FM; (models (Lipman et al., 2022))). These models leverage dynamic transport maps underpinned by the utilization of SDEs or ODEs. Unlike DM, Bridge and Flow Matching relaxes the reliance on a forward diffusion process with an asymptotic convergence to a prior distribution over an infinite time horizon. Moreover, they exhibit a heightened degree of versatility, enabling the construction of transport maps between two arbitrary distributions by drawing

*work done while Tianrong Chen is an intern at Apple

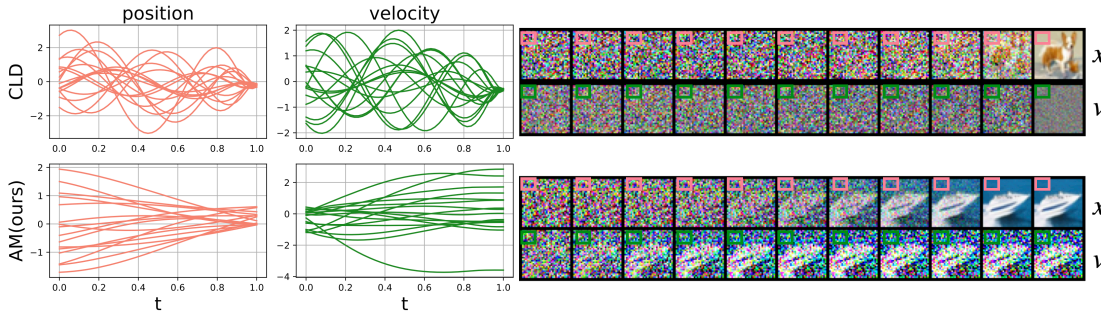


Figure 1: The pixel-wise trajectories comparison with CLD(Dockhorn et al., 2021). Left figures correspond to the trajectories over time w.r.t random sampled 16 pixels, for position and velocity. Our model is able to learn straighter trajectories which is beneficial for reducing sampling complexity.

upon insights from domains such as optimal transport (Pooladian et al., 2023), normalizing flow (Tong et al., 2023b), and optimal control (Liu et al., 2023).

In this paper, we focus on enhancing the sample efficiency of velocity based generative modeling (eg, CLD) by utilizing the Stochastic Optimal Control (SOC) theory. Specifically, we leverage the outcomes of stochastic bridge within the context of linear momentum systems (Chen & Georgiou, 2015) to construct a path measure bridging the data and prior distribution. The resulting path exhibits a more straight position and velocity trajectory compared to CLD (fig.1), making it more amenable to efficient sampling. Within the broader landscape of dynamic generative modeling (ie, ODE/SDE based generative models), data point can often be represented as linear combinations of scaled intermediate data of dynamics and Gaussian noise. In our work, we re-establish this property, enabling the estimation of target data points by leveraging both *state and velocity* information. In the case of DM and FM, the estimation of target data is exclusively reliant on position information, whereas our method incorporates the additional dimension of velocity data, enhancing the precision and comprehensiveness of our estimations. It is also worth noting that our model exhibits the capacity to generate high fidelity images at early time steps (fig.2). In addition, we propose a sampling technique which demonstrates competitive results with small Number of Function Evaluations (NFEs), eg, 5 to 10. Table.1 demonstrates the design differences among aforementioned models. In summary, our paper presents the following contributions:

1. We propose Acceleration Generative Modeling (AGM) which is built on the SOC theory, enabling the favorable trajectories for efficient sampling over 2nd-order momentum dynamics generative modeling such as CLD.
2. As a result of AGM structural characteristics, it becomes possible to estimate a realistic data point at an early time point, a concept we refer to as sampling-hop. This approach not only yields a significant reduction in sampling complexity but also offers a novel perspective on accelerating the sampling in generative modeling by leveraging additional information from the dynamics.
3. We achieve competitive results compared to DM approaches equipped with specifically designed fast sampling techniques on image datasets, particularly in small NFE settings.

2 PRELIMINARY

Notation: Let $\mathbf{x}_t \in \mathbb{R}^d$ and $\mathbf{v}_t \in \mathbb{R}^d$ denote the d -dimensional position and velocity variable of a particle $\mathbf{m}_t = [\mathbf{x}_t, \mathbf{v}_t]^\top \in \mathbb{R}^{2d}$ at time t . We denote the discretized time series as $0 \leq t_0 < \dots < t_n < t_N < 1$. The Wiener Process is denoted as \mathbf{w}_t . The identity matrix is denoted as $\mathbf{I}_d \in \mathbb{R}^{d \times d}$. We define Σ_t as the covariance matrix of \mathbf{x}_t and \mathbf{v}_t at time step t .

2.1 DYNAMICAL GENERATIVE MODELING

The generative modeling approaches rooted in dynamical systems, including ODE and SDE, have garnered significant attention. Here, we present three noteworthy dynamical generative models: Diffusion Model (DM), Flow Matching (FM) and Bridge Matching (BM).

Table 1: Comparison between models in terms of boundary distributions p_0 and p_1 . Our AGM generalizes DM beyond Gaussian priors to phase space, similar to CLD. However, unlike CLD, AGM does not need to converge to the Gaussian at equilibrium which causes curved trajectory(see Fig.1), instead, velocity distribution will be the convolution of data distribution with Gaussian.

Models	DM/FM	CLD	AGM(ours)
$p_0(\cdot)$	$p_{\text{data}}(x)$	$p_{\text{data}}(x) \times \mathcal{N}(\mathbf{0}, \mathbf{I}_d)$	$\mathcal{N}(\mathbf{0}, \Sigma_0 \times \mathbf{I}_{2d})$
$p_1(\cdot)$	$\mathcal{N}(\mathbf{0}, \mathbf{I}_d)$	$\mathcal{N}(\mathbf{0}, \mathbf{I}_d) \times \mathcal{N}(\mathbf{0}, \mathbf{I}_d)$	$p_{\text{data}}(x) \times p_{\text{data}}(x) * \mathcal{N}(\mathbf{0}, \Sigma_0 \otimes \mathbf{I}_{2d})$

Diffusion Model: In the framework of DM, given \mathbf{x}_0 drawn from a data distribution p_{data} , the model proceeds to construct a SDE,

$$d\mathbf{x}_t = f_t(\mathbf{x}_t)dt + g(t)d\mathbf{w}_t \quad \mathbf{x}_0 \sim p_{\text{data}}(\mathbf{x}) \quad (1)$$

whose terminal distributions at $t = 1$ approach an approximate Gaussian, i.e. $\mathbf{x}_1 \sim \mathcal{N}(\mathbf{0}, \mathbf{I}_d)$. This accomplishment is realized through the careful selection of the diffusion coefficient g_t and the base drift $f_t(\mathbf{x}_t)$. It is noteworthy that the time-reversal (Anderson, 1982) of (1) results in another SDE:

$$d\mathbf{x}_t = [f_t(\mathbf{x}_t) - g_t^2 \nabla_{\mathbf{x}} \log p(\mathbf{x}_t, t)] dt + g(t)d\mathbf{w}_t, \quad \mathbf{x}_1 \sim \mathcal{N}(\mathbf{0}, \mathbf{I}_d) \quad (2)$$

where $p(\cdot, t)$ is the marginal density of (1) at time t and $\nabla_{\mathbf{x}} \log p_t$ is known as the score function. SDE (2) can be regarded as the time-reversal of (1) in such a manner that the path-wise measure is almost surely equivalent to the one induced by (1). As a consequence, these two SDEs share identical marginal over time. In practice, it is feasible to analytically sample \mathbf{x}_t given t and \mathbf{x}_0 . Additionally, we can leverage a neural network to learn the score function by regressing scaled Stein Score $\mathbb{E}_{\mathbf{x}_t, t} \|\mathbf{s}_t^\theta(\mathbf{x}_t, t; \theta) - \nabla_{\mathbf{x}} \log p(\mathbf{x}_t, t | \mathbf{x}_0)\|_2^2$ for the purpose of propagating (2). This learned score can then be integrated into the solution of the aforementioned SDE(2) to simulate the generation of data that adheres to the target data distribution from the prior distribution. Meanwhile, (2) also corresponds to an ODE which shares the same path-wise measure:

$$d\mathbf{x}_t = \left[f_t(\mathbf{x}_t) - \frac{1}{2} g_t^2 \nabla_{\mathbf{x}} \log p(\mathbf{x}_t, t) \right] dt, \quad \mathbf{x}_1 \sim \mathcal{N}(\mathbf{0}, \mathbf{I}_d) \quad (3)$$

which motivates the popular sampler introduced in (Zhang & Chen, 2022; Zhang et al., 2022; Bao et al., 2022) to solve the ODE (2) efficiently.

Bridge Matching and Flow Matching: An alternative approach to exploring the time-reversal of a forward noising process involves the concept of 'building bridges' between two distinct distributions $p_0(\cdot)$ and $p_1(\cdot)$. This method entails the learning of a mimicking diffusion process, commonly referred to as bridge matching, as elucidated in previous works (Peluchetti, 2021; Shi et al., 2022). Here we consider the SDE in the form of:

$$d\mathbf{x}_t = \mathbf{v}_t(\mathbf{x}, t)dt + g_t d\mathbf{w}_t \quad s.t. \quad (\mathbf{x}_0, \mathbf{x}_1) \sim \Pi_{0,1}(\mathbf{x}_0, \mathbf{x}_1) := p_0 \times p_1 \quad (4)$$

which is pinned down at an initial and terminal point x_0, x_1 which are independently samples from predefined p_0 and p_1 . This is commonly known as the reciprocal projection of x_0 and x_1 in the literature (Shi et al., 2023; Peluchetti, 2023; Liu et al., 2022; Léonard et al., 2014). The construction of such SDE is accomplished by meticulous design of \mathbf{v}_t . A widely adopted choice for \mathbf{v}_t is $\mathbf{v}_t := (\mathbf{x}_1 - \mathbf{x}_t)/(1 - t)$, which induces the well-known Brownian Bridge (Liu et al., 2023; Somnath et al., 2023). Similar to the approach in DM and owing to the linear structure of the dynamics, one can efficiently estimate this drift by employing a neural network parameterized by weights θ for regression on: $\mathbb{E}_{\mathbf{x}_t, t} \|\mathbf{v}_t^\theta(\mathbf{x}_t, t; \theta) - \mathbf{v}_t(\mathbf{x}_t, t)\|_2^2$ given \mathbf{x}_1 and t . As extensively discussed in previous studies (Liu et al., 2023; Shi et al., 2022), this bridge matching framework takes on the characteristics of FM (Lipman et al., 2022) when the diffusion coefficient g_t tends to zero.

Remark 1. *The practice of constraining a stochastic process to specific initial and terminal conditions is a well-established setup in SOC. From this perspective, one can derive Brownian Bridge, as elaborated in Appendix.C.1 for comprehensive elucidation. It is imperative to note that the SOC framework will serve as the fundamental basis upon which we will develop our algorithm.*

3 ACCELERATION GENERATIVE MODEL

We apply SOC to characterize the twisted trajectory of momentum dynamics induced by CLD(Dockhorn et al., 2021). It becomes evident that the mechanisms encompassing flow matching, diffusion modeling, and Bridge matching collectively facilitate the construction of an estimated target data point, denoted as \mathbf{x}_1 , by utilizing the intermediate state of the dynamics, \mathbf{x}_t . Our additional objective is to expedite the estimation of a plausible \mathbf{x}_1 by incorporating additional dynamics-related information, such as velocity, thereby curtailing the requisite time integration.

In this section, we introduce the proposed method, termed as the Acceleration Generative Model (AGM), rooted in SOC theory. Building upon (Chen & Georgiou, 2015), we extend the framework by incorporating a time-varying diffusion coefficient and accommodating arbitrary boundary conditions, ultimately arriving at an analytical solution suited for the generative modeling. We demonstrate its efficacy in rectifying the trajectory of CLD, concurrently showcasing its aptitude for accurately estimating the target data at an early timestep t_i , thereby enabling expeditious sampling.

As suggested by BM approach, there is a necessity to formulate a trajectory that bridges the two data points sampled from p_0 and p_1 respectively. Desirably, the intermediate trajectory should exhibit optimal characteristics that facilitate smoothness and linearity. This is essential for the ease of simulating the dynamics system to obtain the solution. In our endeavor to tackle this challenge and enhance the estimation of the data point \mathbf{x}_1 by incorporating velocity components, we encapsulate the problem within a SOC framework, specifically formulated in the phase space which reads:

Definition 2 (Stochastic Bridge problem of linear momentum system (Chen & Georgiou, 2015)).

$$\begin{aligned} \min_{\mathbf{a}_t} \int_0^1 \|\mathbf{a}_t\|_2^2 dt + (\mathbf{m}_1 - m_1)^\top \mathbf{R} (\mathbf{m}_1 - m_1) \quad & s.t. \underbrace{\begin{bmatrix} d\mathbf{x}_t \\ d\mathbf{v}_t \end{bmatrix}}_{d\mathbf{m}_t} = \underbrace{\begin{bmatrix} \mathbf{v}_t \\ \mathbf{a}_t(\mathbf{x}_t, \mathbf{v}_t, t) \end{bmatrix}}_{\mathbf{f}(\mathbf{m}, t)} dt + \underbrace{\begin{bmatrix} \mathbf{0} & \mathbf{0} \\ \mathbf{0} & g_t \end{bmatrix}}_{\mathbf{g}_t} d\mathbf{w}_t, \\ \mathbf{m}_0 := \begin{bmatrix} \mathbf{x}_0 \\ \mathbf{v}_0 \end{bmatrix} = \begin{bmatrix} x_0 \\ v_0 \end{bmatrix}, \quad \mathbf{R} = \begin{bmatrix} \mathbf{r} & \mathbf{0} \\ \mathbf{0} & \mathbf{r} \end{bmatrix} \otimes \mathbf{I}_d, \quad x_1 \sim p_{\text{data}}. \end{aligned} \quad (5)$$

In this context, the matrix \mathbf{R} is recognized as the terminal cost matrix, serving to assess the proximity between the propagated \mathbf{m}_1 and the ground truth m_1 at the terminal time $t = 1$. As the parameter \mathbf{r} approaches positive infinity, the trajectory converges toward the state x_1 , prompting a transition to constrained dynamics wherein the system becomes constrained by two predetermined boundaries, namely m_0 and m_1 . This configuration aligns seamlessly with the principles of constructing a feasible bridge, as advocated by the tenets of BM. It is worth noting that this interpolation approach essentially represents a natural extension (Chen & Georgiou, 2015) of the well-established concept of the Brownian Bridge (Revuz & Yor, 2013), which has been employed in trajectory inference (Somnath et al., 2023; Tong et al., 2023a) and image inpainting tasks (Liu et al., 2023) and its connection with Diffusion has been discussed in Liu et al. (2023). Indeed, it is evident that the target velocity lacks a precise definition within this problem, allowing for flexibility in the design space for our approach. To address this, we opt for the linear interpolation of the intermediate point and the target point, represented as $\mathbf{v}_1 = (\mathbf{x}_1 - \mathbf{x}_t)/(1 - t)$, as the chosen terminal velocity, which also is the optimal control in the original space (see Appendix..C.1). This choice is made due to its ability to construct a trajectory characterized by straightness. Conceptually, the acceleration \mathbf{a}_t continually guides the dynamics towards the linear interpolation of the two data points, serving to mitigate the impact of introduced stochasticity. In contrast to previous bridge matching frameworks, the velocity's boundary condition in our approach *varies over time* since it depends on the state \mathbf{x}_t and t . The velocity variable serves solely as an auxiliary component aimed at straightening the trajectories. Regarding this SOC problem formulation, the solution is,

Proposition 3 (Phase Space Brownian Bridge). *When $\mathbf{r} \rightarrow +\infty$, The solution w.r.t optimization problem 5 is,*

$$\mathbf{a}^*(\mathbf{m}_t, t) = g_t^2 P_{11} \left(\frac{\mathbf{x}_1 - \mathbf{x}_t}{1 - t} - \mathbf{v}_t \right) \quad \text{where :} \quad P_{11} = \frac{-4}{g_t^2(t-1)}. \quad (6)$$

Proof. Please see Appendix.C.2. □

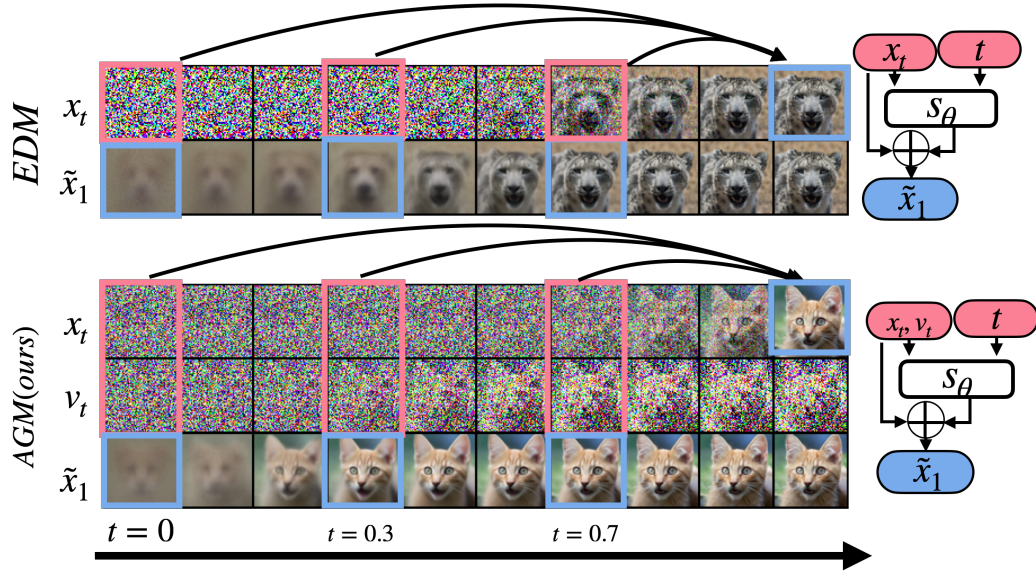


Figure 2: Data estimation comparison with EDM (Karras et al., 2022). When the network is endowed with supplementary velocity, AGM gains the capacity to estimate the target data point during the early stages of the trajectory. One can use estimated image \tilde{x}_1 at $t_i < t_N$ as generated results and allocate more NFE between time $[0, t_i]$ which results to smaller discretization error.

Remark 4. P_{11} denotes the second diagonal component in the matrix P_t , a solution derived from the Lyapunov equation (see Lemma.6), serving as an implicit representation of the optimality of the control. This value is dependent upon the uncontrolled dynamics, where \mathbf{a}_t is set to the zero vector in (5), and will vary accordingly when uncontrolled dynamics change.

3.1 TRAINING

By plugging the optimal control (6) back to the dynamics (5), we can obtain the desired SDE. As been suggested by (Song et al., 2020b; Dockhorn et al., 2021), such SDE has a corresponding probabilistic ODE which shares the same marginal over time in which the drift term will have an additional score term $\nabla_{\mathbf{v}} \log p(\mathbf{m}_t, t)$. Here we summarize the force term for SDE and ODE as:

$$\begin{aligned} \begin{bmatrix} d\mathbf{x}_t \\ d\mathbf{v}_t \end{bmatrix} &= \begin{bmatrix} \mathbf{v}_t \\ \mathbf{F}_t \end{bmatrix} dt + \begin{bmatrix} \mathbf{0} & \mathbf{0} \\ \mathbf{0} & g_t \end{bmatrix} d\mathbf{w}_t \quad \text{s.t. } \mathbf{m}_0 := \begin{bmatrix} \mathbf{x}_0 \\ \mathbf{v}_0 \end{bmatrix} \sim \mathcal{N}(\boldsymbol{\mu}_0, \boldsymbol{\Sigma}_0), \\ \text{Bridge Matching SDE: } \mathbf{F}_t &:= \mathbf{F}_t^b(\mathbf{m}_t, t) \equiv \mathbf{a}_t^*(\mathbf{m}_t, t), \quad g(t) := g(t), \quad (7) \\ \text{Probabilistic ODE: } \mathbf{F}_t &:= \mathbf{F}_t^p(\mathbf{m}_t, t) \equiv \mathbf{a}_t^*(\mathbf{m}_t, t) - \frac{1}{2} g_t^2 \nabla_{\mathbf{v}} \log p(\mathbf{m}, t), \quad g(t) := 0. \end{aligned}$$

Henceforth, we refer to the dynamics associated with the Bridge Matching SDE as AGM-SDE, and its corresponding ODE counterpart as AGM-ODE. Meanwhile, the linearity of the system implies the intermediate state \mathbf{m}_t and the close form solution of score term are analytically available. In particular, the mean $\boldsymbol{\mu}_t$ and covariance matrix $\boldsymbol{\Sigma}_t$ of the intermediate marginal $p_t(\mathbf{m}_t | \mathbf{x}_1) = \mathcal{N}(\boldsymbol{\mu}_t, \boldsymbol{\Sigma}_t)$ of such a system can be analytically computed with $\boldsymbol{\Sigma}_t = \begin{bmatrix} \Sigma_t^{xx} & \Sigma_t^{xv} \\ \Sigma_t^{xv} & \Sigma_t^{vv} \end{bmatrix} \otimes \mathbf{I}_d$, and $\boldsymbol{\mu}_t = \begin{bmatrix} \boldsymbol{\mu}_t^x \\ \boldsymbol{\mu}_t^v \end{bmatrix}$, provided we have the boundary conditions $\boldsymbol{\mu}_0$ and $\boldsymbol{\Sigma}_0$ in place, as outlined in Särkkä & Solin (2019). Please see Appendix.C.3 for detail. In order to sample from such multi-variate Gaussian, one need to decompose the covariance matrix by Cholesky decomposition, and \mathbf{m}_t is reparametrized as:

$$\mathbf{m}_t = \boldsymbol{\mu}_t + \mathbf{L}_t \boldsymbol{\epsilon} = \boldsymbol{\mu}_t + \begin{bmatrix} L_t^{xx} \boldsymbol{\epsilon}_0 \\ L_t^{xv} \boldsymbol{\epsilon}_0 + L_t^{vv} \boldsymbol{\epsilon}_1 \end{bmatrix}, \quad \nabla_{\mathbf{v}} \log p_t := -\ell_t \boldsymbol{\epsilon}_1 \quad (8)$$

where $\boldsymbol{\Sigma}_t = \mathbf{L}_t \mathbf{L}_t^T$, $\boldsymbol{\epsilon} = \begin{bmatrix} \boldsymbol{\epsilon}_0 \\ \boldsymbol{\epsilon}_1 \end{bmatrix} \sim \mathcal{N}(\mathbf{0}, \mathbf{I}_{2d})$ and $\ell_t = \sqrt{\frac{\Sigma_t^{xx}}{\Sigma_t^{xx} \Sigma_t^{vv} - (\Sigma_t^{xv})^2}}$.

Parameterization: The Force term can be represented as a composite of the data point and Gaussian noise. Specifically,

$$\mathbf{a}^*(\mathbf{m}_t, t) = 4\mathbf{x}_1(1-t)^2 - g_t^2 P_{11} \left[\left(\frac{L_t^{xx}}{1-t} + L_t^{xv} \right) \epsilon_0 + L_t^{vv} \epsilon_1 \right].$$

We express the force term as $\mathbf{F}_t^\theta = \mathbf{s}_t^\theta \cdot \mathbf{z}_t$. Here, \mathbf{z}_t assumes the role of regulating the output of the network \mathbf{s}_t^θ , ensuring that the variance of the network output is normalized to unity. For the detailed formulation of the normalizer \mathbf{z}_t , please refer to Appendix.C.8. In a manner similar to the BM approach, one can formulate the objective function for regressing the force term as follows:

$$\min_{\theta} \mathbb{E}_{t \in [0,1]} \mathbb{E}_{\mathbf{x}_1 \sim p_{\text{data}}} \mathbb{E}_{\mathbf{m}_t \sim p_t(\mathbf{m}_t | \mathbf{x}_1)} \lambda(t) [\|\mathbf{F}_t^\theta(\mathbf{m}_t, t; \theta) - \mathbf{F}_t(\mathbf{m}_t, t)\|_2^2] \quad (9)$$

Where $\lambda(t)$ is known as the reweight of the objective function across the time horizon. We defer the derivation of ℓ_t and the presentation of \mathbf{L}_t , $\lambda(t)$ and \mathbf{a}_t in Appendix.C.

3.2 SAMPLING FROM AGM

Once the parameterized force term \mathbf{F}_t^θ is trained, we are ready to simulate the dynamics to generate the samples by plugging it back to the dynamics (15). One can use any type of SDE or ODE sampler to propagate the learnt system. Here we list our choice of sampler for AGM-SDE and AGM-ODE.

Stochastic Sampler: To simulate the SDE, prior works are majorly relying on Euler-Maruyama(EM) (Kloeden et al., 1992) and related methods. We adopt the Symmetric Splitting Sampler(SSS) from Dockhorn et al. (2021) in our AGM-SDE. This selection is based on the compelling performance it offers when dealing with momentum systems.

Deterministic Sampler: It is imperative to acknowledge that this system is inherently underactuated because the force term is exclusively injected into the velocity component, while velocity serves as the driving factor for the position—a variable of primary interest in generative modeling context. More specifically, at time step t_i , the impact of force does not immediately manifest in the position but rather takes effect at a subsequent time step, denoted as t_{i+1} after discretizing time horizon. At time t_0 , it becomes undesirable to propagate the state \mathbf{x}_0 using an initially uncontrolled velocity over an extended time interval δ_0 . The presence of this delay phenomenon can also exert an influence when the time interval δ_t is large, thereby impeding our ability to reduce the NFE during sampling. We propose the adoption of an Exponential Integrator (EI) approach, as elaborated in Zhang & Chen (2022). Empirical evidence suggests that this method aligns well with our model. We provide an illustrative example of how the AGM-ODE, in conjunction with the EI technique, can be employed to inject the learnt network into both velocity and position channels simultaneously:

$$\begin{bmatrix} \mathbf{x}_{t_{i+1}} \\ \mathbf{v}_{t_{i+1}} \end{bmatrix} = \Phi(t_{i+1}, t_i) \begin{bmatrix} \mathbf{x}_t \\ \mathbf{v}_t \end{bmatrix} + \sum_{j=0}^w \begin{bmatrix} \int_{t_i}^{t_{i+1}} (t_{i+1} - \tau) \mathbf{z}_\tau \cdot \mathbf{M}_{i,j}(\tau) d\tau \cdot \mathbf{s}_t^\theta(\mathbf{m}_{t_{i-j}}, t_{i-j}) \\ \int_{t_i}^{t_{i+1}} \mathbf{z}_\tau \cdot \mathbf{M}_{i,j}(\tau) d\tau \cdot \mathbf{s}_t^\theta(\mathbf{m}_{t_{i-j}}, t_{i-j}) \end{bmatrix} \quad (10)$$

Where $\mathbf{M}_{i,j}(\tau) = \prod_{k \neq j} \left(\frac{\tau - t_{i-k}}{t_{i-j} - t_{i-k}} \right)$, and $\Phi(t, s) = \begin{bmatrix} 1 & t-s \\ 0 & 1 \end{bmatrix}$.

In Eq.10, $\Phi(s, t)$ denotes the transition matrix for our system, while $\mathbf{M}_{i,j}(\tau)$ represents the w -order multistep coefficient (Hochbruck & Ostermann, 2010). For a comprehensive derivation of these terms, please refer to Appendix.C.9. It is worth noting that the mapping of \mathbf{s}_θ into both the position and velocity channels significantly emulates the errors introduced by discretization delays.

Sampling-hop: In the context of CLD (Dockhorn et al., 2021), their focus is on estimating the score function with respect to velocity, which essentially corresponds to estimating scaled ϵ_1 in our notation. This estimation process restrains them from making predictions of the data from the current state and velocity alone. Remarkably, our observations have unveiled that when the network is equipped with additional velocity information, it acquires the capability to estimate the target data point during the early stages of the trajectory, as illustrated in fig.2. This estimation can be seamlessly integrated into AGM-SDE and AGM-ODE and we name it sampling-hop. Specifically,

Proposition 5 (Sampling-Hop). *The estimated data point \mathbf{x}_1 can be represented as*

$$\tilde{\mathbf{x}}_1^{SDE} = \frac{(1-t)(\mathbf{F}_t^\theta + \mathbf{v}_t)}{g_t^2 P_{11}} + \mathbf{x}_t, \text{ or } \tilde{\mathbf{x}}_1^{ODE} = \frac{\mathbf{F}_t^\theta + g_t^2 P_{11}(\alpha_t \mathbf{x}_t + \beta_t \mathbf{v}_t)}{4(t-1)^2 + g_t^2 P_{11}(\alpha_t \mu_t^x + \beta_t \mu_t^v)} \quad (11)$$

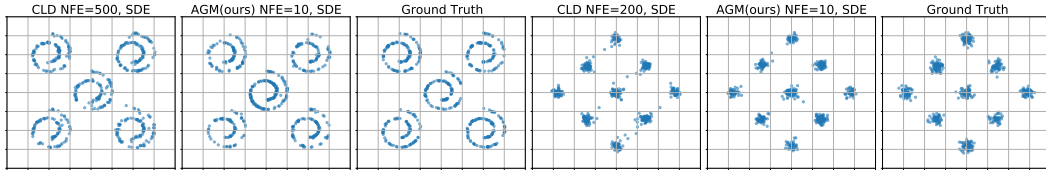


Figure 4: The comparison with CLD(Dockhorn et al., 2021) using same network and stochastic sampler SSS, for Multi-Swiss-Roll and Mixture of Gaussian datasets. We achieve visually better results with one order less NFEs.

for AGM-SDE and AGM-ODE dynamics respectively, and $\beta_t = L_t^{vv} + \frac{1}{2P_{11}}, \alpha_t = \frac{(\frac{L_t^{xx}}{1-t} + L_t^{xv}) - \beta_t L_t^{xv}}{L_t^{xx}}$.

Proof. See Appendix.C.10 \square

This property empowers us to allocate the NFE budget selectively within the time interval $t \in [0, t_i]$, where $t_i < t_N$, effectively reducing the discretization error while maintaining the sampling quality. This insight paves the way for efficient low NFE sampling strategies later. Here we summarized the training and sampling procedure of our method in Algorithm.1 and Algorithm.2 respectively.

Algorithm 1 Training

```

1: Input: data distribution  $p_{\text{data}}(\cdot)$ 
2: while not converge do
3:    $t \sim \mathcal{U}([0, 1]), \mathbf{x}_1 \sim p_{\text{data}}(\mathbf{x}_1)$ 
4:    $\mathbf{m}_t \sim q_t(\mathbf{m}_t | \mathbf{x}_1)$  according to eq.8
5:   Compute the loss using eq.9.
6:   Take gradient descent with respect to
       $\mathbf{F}(\mathbf{m}_t, t; \theta)$ .
7: end while

```

Algorithm 2 Sampling

```

1: Input: trained  $\mathbf{F}(\cdot, \cdot; \theta)$ , discretized time
   step  $[t_0, \dots, t_i]$ , Choose the sampler from
   [SSS(SDE), EI(ODE)].
2: Sample  $\mathbf{m}_0 \sim p_0(\mathbf{m}; \mu_0, \Sigma_0)$ 
3: for  $n = 0$  to  $i$  do
4:   estimate  $\mathbf{F}_t^\theta(\mathbf{m}_{t_n}, t_n)$ 
5:    $\mathbf{m}_{t_{n+1}} = \text{Sampler}(\mathbf{m}_{t_n}, F_{t_n}^\theta, t_n)$ 
6: end for

```

4 EXPERIMENTAL RESULTS

Architectures and Hyperparameters: We parameterize $\mathbf{s}_t^\theta(\cdot, \cdot; \theta)$ using modified NCSN++ model as provided in Karras et al. (2022). We employ six input channels, accounting for both position and velocity variables, as opposed to the standard three channels used in the CIFAR-10 (Krizhevsky et al., 2009), AFHQv2 (Choi et al., 2020) and ImageNet (Deng et al., 2009) which leads to a negligible increase of network parameters. For the purpose of comparison with CLD in the toy dataset, we adopt the same ResNet-based architecture utilized in CLD. Throughout all of our experiments, we maintain a monotonically decreasing diffusion coefficient, given by $g(t) = 3(1 - t)$. For the detailed experimental setup, please refer further to Appendix.D.

Evaluation: To assess the performance and the sampling speed of various algorithms, we employ the Fréchet Inception Distance score (FID; Heusel et al. (2017)) and the Number of Function Evaluations (NFE) as our metrics. For FID evaluation, we utilize reference statistics of all datasets obtained from EDM (Karras et al., 2022) and use 50k generated samples to evaluate. Additionally, we re-evaluate the FID of CLD and EDM using the same reference statistics to ensure consistency in our comparisons. For all other reported values, we directly source them from respective referenced papers.

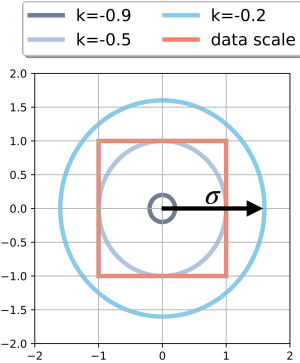


Figure 3: The standard deviation σ of the terminal marginal for uncontrolled dynamics. We empirically selected the hyperparameter $k = -0.2$. This choice induces a terminal marginal distribution with σ that covers the data range with uncontrolled dynamics.

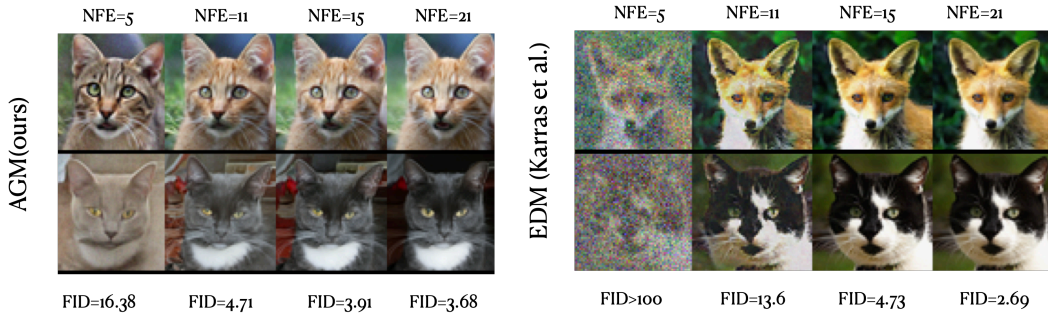


Figure 5: Comparison with EDM (Karras et al., 2022) on AFHQv2 dataset. AGM-ODE exhibits superior generative performance when NFE is exceedingly low, owing to its unique dynamics architecture that incorporates velocity when predicting the estimated data point.

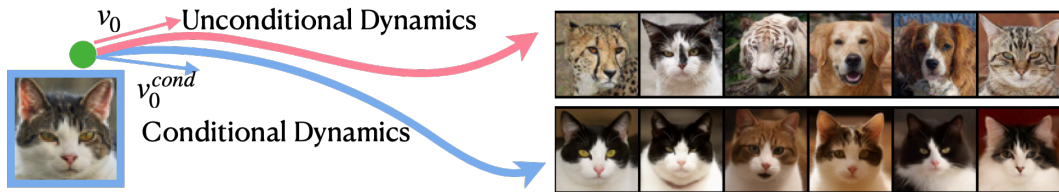


Figure 6: We showcase that AGM can generate conditional results from an unconditional model by injecting the conditional information into the velocity \mathbf{v}_0 , thus leading to new initial velocity \mathbf{v}_0^{cond} .

Selection of Σ_0 : The choice of initial covariance Σ_0 directly influences the path measure of the trajectory. In our case, we set $\Sigma_0 := \begin{bmatrix} 1 & k \\ k & 1 \end{bmatrix}$ with hyperparameter k . We observe that trajectories tend to exhibit pronounced curvature under specific conditions: when the k is positive, the absolute value of the position is large. This behavior is particularly noticeable when dealing with images, where the data scale ranges from -1 to 1. We aim for favorable uncontrolled dynamics, as this can potentially lead to better-controlled dynamics. Our strategy is to design k in such a way that the marginal distribution of uncontrolled dynamics at $t_N = 1$ effectively covers the range of image data values meanwhile k keeps negative. We can express the marginal of uncontrolled dynamics by leveraging the transition matrix $\Phi(1, 0)$, which gives us $\mathbf{x}_1 := \mathbf{x}_0 + \mathbf{v}_0$. Figure 3 illustrates the standard deviation of \mathbf{x}_1 for various values of k . Based on our empirical observations, we choose $k = -0.2$ for all experiments, as it effectively covers the data range. The subsequent controlled dynamics (eq.15) will be constructed based on such desired uncontrolled dynamics as established.

Stochastic Sampling: In our experiments, we emphasize the advantages of employing the AGM-SDE in comparison to CLD. Firstly, we demonstrate that our model exhibits superior performance when NFE is significantly lower than that of CLD, particularly in toy dataset scenarios. For evaluation, we utilized the multi-modal Mixture of Gaussian and Multi-Swiss-Roll datasets. The results obtained from the toy dataset, as shown in Fig.4, demonstrate that AGM-SDE is capable of generating data that closely aligns with the ground truth, while requiring NFE that is around one order of magnitude lower than CLD. Furthermore, our findings reveal that AGM-SDE outperforms CLD in the context of CIFAR-10 image generation tasks, especially when faced with limited NFE, as illustrated in Table 2.

Deterministic Sampling: Next, we validate our algorithm on high-dimensional image generation with a deterministic sampler. We provide uncurated samples from CIFAR-10, AFHQv2 and ImageNet-64 with varying NFE in Appendix.E. Regarding the quantitative evaluation, Table.3 and Table.4 summarize the FID together with NFE used for sampling on CIFAR-

Table 2: $FID \downarrow$ Comparison with CLD(Dockhorn et al., 2021) using same SSS Sampler on CIFAR-10.

NFE \downarrow	CLD-SDE	AGM-SDE
20	>100	7.9
50	19.93	3.21
150	2.99	2.68
1000	2.44	2.46

Table 3: Unconditional CIFAR-10 generative performance

	Model Name	NFE↓	FID↓
ODE	EDM (Karras et al., 2022)	35	1.84
	CLD+EI (Zhang et al., 2022)	50	2.26
	FM-OT (Lipman et al., 2022)	142	6.35
	AGM-ODE(ours)	50	2.46
SDE	VP (Song et al., 2020b)	1000	2.66
	VE (Song et al., 2020b)	1000	2.43
	CLD (Dockhorn et al., 2021)	1000	2.44
	AGM-SDE(ours)	1000	2.46

Table 4: Unconditional ImageNet-64 generative performance

Model	NFE↓	FID↓
DDPM(Ho et al., 2020)	264	17.36
FM-OT(Lipman et al., 2022)	138	14.45
MFM(Pooladian et al., 2023)	132	11.82
MFM(Pooladian et al., 2023)	40	12.97
AGM-ODE(ours)	40	10.97
AGM-ODE(ours)	20	12.55

Table 5: Performance comparing with fast sampling algorithm using FID↓ metric on CIFAR-10

Dynamics Order	Model Name	NFE↓	5	10	20
1st order dynamics	EDM (Karras et al., 2022)	> 100	15.78	2.23	
	VP+EI (Zhang & Chen, 2022)	15.37	4.17	3.03	
	DDIM (Song et al., 2020a)	26.91	11.14	3.50	
	Analytic-DPM(Bao et al., 2022)	51.47	14.06	6.74	
2nd order dynamics	CLD+EI (Zhang et al., 2022)	N/A	13.41	3.39	
	AGM-ODE(ours)	11.93	4.60	2.60	

10 and ImageNet-64. Notably, AGM-ODE achieves 2.46 FID score with 50 NFE on CIFAR-10, and 10.97 FID score with 40 NFE in ImageNet-64 which outperforms the existing dynamical generative modelings.

We underscore the effectiveness of sampling-hop, especially when faced with a constrained NFE budget, in comparison to baselines. We validate it on the CIFAR-10 and AFHQv2 dataset respectively. Fig.5 illustrates that AGM-ODE is able to generate plausible images even when NFE= 5 and outperforms EDM(Karras et al., 2022) when NFE is extremely small (NFE<15) visually and numerically on AFHQv2 dataset. We also compare with other fast sampling algorithms built upon DM in table.5 on CIFAR-10 dataset where AGM-ODE demonstrates competitive performance. Notably, AGM-ODE outperforms the baseline CLD with the same EI sampler by a large margin. We suspect that the improvement is based on the rectified trajectory which is more friendly for the ODE solver.

Conditional Generation We showcase the capability of AGM to generate conditional samples using an unconditional model (fig.6) by incorporating conditional information into the prior velocity variable \mathbf{v}_0 . Instead of employing a randomly sampled \mathbf{v}_0 , we use a linear combination of \mathbf{v}_0 and the desired velocity $\mathbf{v}_1 = (\mathbf{x}_1 - \mathbf{x}_{t_0})/(1-t_0)$, where \mathbf{x}_1 is conditioned data. Thus, at timestep t_0 , the initial velocity is defined as $\mathbf{v}_0^{cond} := (1-\xi)\mathbf{v}_0 + \xi\mathbf{v}_1$, with ξ serving as a mixing coefficient. Fig.6 shows that AGM can generate conditional data *without* augmentation and additional fine-tuning.

5 CONCLUSION AND LIMITATION

In this paper, we introduce a novel Acceleration Generative Modeling (AGM) framework rooted in SOC theory. Within this framework, we devise more favorable, straight trajectories for the momentum system. Leveraging the intrinsic characteristics of the momentum system, we capitalize on additional velocity to expedite the sampling process by using the sampling-hop technique, significantly reducing the time required to converge to accurate predictions of realistic data points. Our experimental results, conducted on both toy and image datasets in unconditional generative tasks, demonstrate promising outcomes for fast sampling.

However, it is essential to acknowledge that our approach’s performance lags behind state-of-the-art methods in scenarios with sufficient NFE. This observation suggests avenues for enhancing AGM performance. Such improvements could be achieved by enhancing the training quality through the

adoption of techniques proposed in Karras et al. (2022) including data augmentation, fine-tuned noise scheduling, and network preconditioning, among others.

REFERENCES

Brian DO Anderson. Reverse-time diffusion equation models. *Stochastic Processes and their Applications*, 12(3):313–326, 1982.

Fan Bao, Chongxuan Li, Jun Zhu, and Bo Zhang. Analytic-dpm: an analytic estimate of the optimal reverse variance in diffusion probabilistic models. *arXiv preprint arXiv:2201.06503*, 2022.

Yongxin Chen and Tryphon Georgiou. Stochastic bridges of linear systems. *IEEE Transactions on Automatic Control*, 61(2):526–531, 2015.

Yunjey Choi, Youngjung Uh, Jaejun Yoo, and Jung-Woo Ha. Stargan v2: Diverse image synthesis for multiple domains. In *Proceedings of the IEEE/CVF conference on computer vision and pattern recognition*, pp. 8188–8197, 2020.

Jia Deng, Wei Dong, Richard Socher, Li-Jia Li, Kai Li, and Li Fei-Fei. Imagenet: A large-scale hierarchical image database. In *2009 IEEE conference on computer vision and pattern recognition*, pp. 248–255. Ieee, 2009.

Prafulla Dhariwal and Alex Nichol. Diffusion models beat gans on image synthesis. *arXiv preprint arXiv:2105.05233*, 2021.

Tim Dockhorn, Arash Vahdat, and Karsten Kreis. Score-based generative modeling with critically-damped langevin diffusion. *arXiv preprint arXiv:2112.07068*, 2021.

Ulrich G Haussmann and Etienne Pardoux. Time reversal of diffusions. *The Annals of Probability*, pp. 1188–1205, 1986.

Martin Heusel, Hubert Ramsauer, Thomas Unterthiner, Bernhard Nessler, and Sepp Hochreiter. Gans trained by a two time-scale update rule converge to a local nash equilibrium. *Advances in neural information processing systems*, 30, 2017.

Jonathan Ho, Ajay Jain, and Pieter Abbeel. Denoising diffusion probabilistic models. *arXiv preprint arXiv:2006.11239*, 2020.

Marlis Hochbruck and Alexander Ostermann. Exponential integrators. *Acta Numerica*, 19:209–286, 2010.

The MathWorks Inc. Matlab version: 9.13.0 (r2022b), 2022. URL <https://www.mathworks.com>.

HJ Kappen. Stochastic optimal control theory. *ICML, Helsinki, Radbound University, Nijmegen, Netherlands*, 2008.

Tero Karras, Miika Aittala, Timo Aila, and Samuli Laine. Elucidating the design space of diffusion-based generative models. *Advances in Neural Information Processing Systems*, 35:26565–26577, 2022.

Donald E Kirk. *Optimal control theory: an introduction*. Courier Corporation, 2004.

Peter E Kloeden, Eckhard Platen, Peter E Kloeden, and Eckhard Platen. *Stochastic differential equations*. Springer, 1992.

Alex Krizhevsky, Geoffrey Hinton, et al. Learning multiple layers of features from tiny images. 2009.

Christian Léonard, Sylvie Rœlly, and Jean-Claude Zambrini. Reciprocal processes. a measure-theoretical point of view. 2014.

Yaron Lipman, Ricky TQ Chen, Heli Ben-Hamu, Maximilian Nickel, and Matt Le. Flow matching for generative modeling. *arXiv preprint arXiv:2210.02747*, 2022.

Guan-Horng Liu, Arash Vahdat, De-An Huang, Evangelos A Theodorou, Weili Nie, and Anima Anandkumar. I2sb: Image-to-image schrödinger bridge. *arXiv preprint arXiv:2302.05872*, 2023.

Xingchao Liu, Lemeng Wu, Mao Ye, and Qiang Liu. Let us build bridges: Understanding and extending diffusion generative models. *arXiv preprint arXiv:2208.14699*, 2022.

Ilya Loshchilov and Frank Hutter. Decoupled weight decay regularization. *arXiv preprint arXiv:1711.05101*, 2017.

Bernt Øksendal. Stochastic differential equations. In *Stochastic differential equations*, pp. 65–84. Springer, 2003.

Stefano Peluchetti. Non-denoising forward-time diffusions. 2021.

Stefano Peluchetti. Diffusion bridge mixture transports, schrödinger bridge problems and generative modeling. *arXiv preprint arXiv:2304.00917*, 2023.

Aram-Alexandre Pooladian, Heli Ben-Hamu, Carles Domingo-Enrich, Brandon Amos, Yaron Lipman, and Ricky Chen. Multisample flow matching: Straightening flows with minibatch couplings. *arXiv preprint arXiv:2304.14772*, 2023.

Daniel Revuz and Marc Yor. *Continuous martingales and Brownian motion*, volume 293. Springer Science & Business Media, 2013.

Simo Särkkä and Arno Solin. *Applied stochastic differential equations*, volume 10. Cambridge University Press, 2019.

Yuyang Shi, Valentin De Bortoli, George Deligiannidis, and Arnaud Doucet. Conditional simulation using diffusion schrödinger bridges. In *Uncertainty in Artificial Intelligence*, pp. 1792–1802. PMLR, 2022.

Yuyang Shi, Valentin De Bortoli, Andrew Campbell, and Arnaud Doucet. Diffusion schrödinger bridge matching. *arXiv preprint arXiv:2303.16852*, 2023.

Vignesh Ram Somnath, Matteo Pariset, Ya-Ping Hsieh, Maria Rodriguez Martinez, Andreas Krause, and Charlotte Bunne. Aligned diffusion schrödinger bridges. *arXiv preprint arXiv:2302.11419*, 2023.

Jiaming Song, Chenlin Meng, and Stefano Ermon. Denoising diffusion implicit models. *arXiv preprint arXiv:2010.02502*, 2020a.

Yang Song, Jascha Sohl-Dickstein, Diederik P Kingma, Abhishek Kumar, Stefano Ermon, and Ben Poole. Score-based generative modeling through stochastic differential equations. *arXiv preprint arXiv:2011.13456*, 2020b.

Yang Song, Conor Durkan, Iain Murray, and Stefano Ermon. Maximum likelihood training of score-based diffusion models. *arXiv e-prints*, pp. arXiv–2101, 2021.

Alexander Tong, Nikolay Malkin, Kilian Fatras, Lazar Atanackovic, Yanlei Zhang, Guillaume Huguet, Guy Wolf, and Yoshua Bengio. Simulation-free schrödinger bridges via score and flow matching. *arXiv preprint arXiv:2307.03672*, 2023a.

Alexander Tong, Nikolay Malkin, Guillaume Huguet, Yanlei Zhang, Jarrid Rector-Brooks, Kilian Fatras, Guy Wolf, and Yoshua Bengio. Improving and generalizing flow-based generative models with minibatch optimal transport. In *ICML Workshop on New Frontiers in Learning, Control, and Dynamical Systems*, 2023b.

Jiongmin Yong and Xun Yu Zhou. *Stochastic controls: Hamiltonian systems and HJB equations*, volume 43. Springer Science & Business Media, 1999.

Qinsheng Zhang and Yongxin Chen. Fast sampling of diffusion models with exponential integrator. *arXiv preprint arXiv:2204.13902*, 2022.

Qinsheng Zhang, Molei Tao, and Yongxin Chen. gddim: Generalized denoising diffusion implicit models. *arXiv preprint arXiv:2206.05564*, 2022.

Qinsheng Zhang, Jiaming Song, and Yongxin Chen. Improved order analysis and design of exponential integrator for diffusion models sampling. *arXiv preprint arXiv:2308.02157*, 2023.

A SUPPLEMENTARY SUMMARY

We state the assumptions in Appendix.B. We provide the technique details appearing in Section.3 at Appendix.C. The details of the experiments can be found in Appendix.D. The visualization of generated figures can be found in Appendix.E.

B ASSUMPTIONS

We will use the following assumptions to construct the proposed method. These assumptions are adopted from stochastic analysis for SGM (Song et al., 2021; Yong & Zhou, 1999; Anderson, 1982),

- (i) p_0 and p_1 with finite second-order moment.
- (ii) g_t is continuous functions, and $|g(t)|^2 > 0$ is uniformly lower-bounded w.r.t. t .
- (iii) $\forall t \in [0, 1]$, we have $\nabla_{\mathbf{v}} \log p_t(\mathbf{m}_t, t)$ Lipschitz and at most linear growth w.r.t. \mathbf{x} and \mathbf{v} .

Assumptions (i) (ii) are standard conditions in stochastic analysis to ensure the existence-uniqueness of the SDEs; hence also appear in SGM analysis (Song et al., 2021).

C TECHNIQUE DETAILS IN SECTION.3

C.1 BROWNIAN BRIDGE AS THE SOLUTION OF STOCHASTIC OPTIMAL CONTROL

We adopt the presentation form Kappen (2008). We consider the control problem:

$$\begin{aligned} \min_{\mathbf{v}_t} \int_{t_0}^1 \frac{1}{2} \|\mathbf{v}_t\|_2^2 dt + \frac{\mathbf{r}}{2} \|\mathbf{x}_1 - \mathbf{x}_0\|_2^2 \\ \text{s.t. } d\mathbf{x}_t = \mathbf{v}_t dt, \quad \mathbf{x}_0 = \mathbf{x}_0 \end{aligned}$$

Where \mathbf{r} is the terminal cost coefficient. According to Pontryagin Maximum Principle (PMP;Kirk (2004)) recipe, one can construct the Hamiltonian:

$$H(t, \mathbf{x}, \mathbf{v}, \gamma) = -\frac{1}{2} \|\mathbf{v}_t\|_2^2 + \gamma \mathbf{v}_t$$

Hence the optimized Hamiltonian is:

$$H(t, \mathbf{x}, \mathbf{v}, \gamma)^* = \frac{1}{2} \gamma^2, \quad \text{where } \mathbf{v}_t = \gamma$$

Then we solve the Hamiltonian equation of motion:

$$\begin{aligned} \frac{d\mathbf{x}_t}{dt} &= \frac{\partial H^*}{\partial \gamma} = \gamma \\ \frac{d\gamma}{dt} &= \frac{\partial H^*}{\partial \mathbf{x}} = 0 \\ \text{where } \mathbf{x}_0 &= \mathbf{x}_0 \quad \text{and} \quad \gamma_1 = -\mathbf{r} \cdot (\mathbf{x}_1 - \mathbf{x}_0) \end{aligned}$$

One can notice that the solution for γ_t is the constant $\gamma_t = \gamma = -\mathbf{r} \cdot (\mathbf{x}_1 - \mathbf{x}_0)$, hence the solution for \mathbf{x}_t is $\mathbf{x}_t = \mathbf{x}_0 + \gamma t$.

$$\begin{aligned} \gamma &= -\mathbf{r}(\mathbf{x}_1 - \mathbf{x}_0) = -\mathbf{r}(\mathbf{x}_0 + (1 - t_0)\gamma - \mathbf{x}_1) \\ \rightarrow \mathbf{v}_t^* &:= \gamma = \frac{\mathbf{r}(\mathbf{x}_1 - \mathbf{x}_0)}{1 + \mathbf{r}(1 - t_0)} \end{aligned}$$

When $\mathbf{r} \rightarrow +\infty$, we arrive the optimal control as $\mathbf{v}_t^* = \frac{\mathbf{x}_1 - \mathbf{x}_0}{1 - t_0}$. Due to certainty equivalence, this is also the optimal control law for

$$d\mathbf{x}_t = \mathbf{v}_t dt + d\mathbf{w}_t$$

By plugging it back into the dynamics, we obtain the well-known Brownian Bridge:

$$d\mathbf{x}_t = \frac{\mathbf{x}_1 - \mathbf{x}_t}{1-t} dt + g_t d\mathbf{w}_t$$

C.2 PROOF OF PROPOSITION.3

Lemma 6. *The solution of following Lyapunov equation,*

$$\dot{\mathbf{P}} = \mathbf{A}\mathbf{P} + \mathbf{P}\mathbf{A}^T - \mathbf{g}\mathbf{g}^T \quad (12)$$

with terminal condition

$$\mathbf{P}_T = \begin{bmatrix} 0 & 0 \\ 0 & R \end{bmatrix} \quad (13)$$

is given by

$$\mathbf{P}_t = \begin{bmatrix} r(t-1)^2 - \frac{1}{3}g^2(t-1)^3 & r(t-1) - \frac{1}{2}g^2(t-1)^2 \\ r(t-1) - \frac{1}{2}g^2(t-1)^2 & g^2(1-t) + r \end{bmatrix}$$

and the inverse of \mathbf{P}_t is,

$$\mathbf{P}_t^{-1} = \frac{1}{g^2(-4r + g^2(t-1))(t-1)} \begin{bmatrix} \frac{12(r-g^2(t-1))}{(t-1)^2} & \frac{6(-2r+g^2(t-1))}{t-1} \\ \frac{6(-2r+g^2(-1+t))}{t-1} & 12r - 4g^2(t-1) \end{bmatrix}$$

When $\mathbf{A} = \begin{bmatrix} 0 & 1 \\ 0 & 0 \end{bmatrix}$, $\mathbf{g} = \begin{bmatrix} 0 \\ g \end{bmatrix}$ and $R = r\mathbf{I}$.

Thus,

$$\begin{aligned} P_{10} &= \frac{-12r + 6g^2(t-1)}{g^2[-4r + g^2(t-1)](t-1)^2} = \frac{-12r}{g^2[-4r + g^2(t-1)](t-1)^2} + \frac{6}{[-4r + g^2(t-1)](t-1)} \\ P_{11} &= \frac{12r - 4g^2(t-1)}{g^2[-4r + g^2(t-1)](t-1)} = \frac{12r}{g^2[-4r + g^2(t-1)](t-1)} - \frac{4}{[-4r + g^2(t-1)]} \end{aligned}$$

Proof. One can plug in the solution of \mathbf{P}_t into the Lyapunov equation \mathbf{P}_t and it validates \mathbf{P}_t is indeed the solution.

Remark 7. *Here we provide a general form when the terminal condition of the Lyapunov function is not a zero matrix. It explicitly means that it allows that the velocity does not necessarily need to converge to the exact predefined \mathbf{v}_1 . It will have the same results as shown in the paper by setting $r = 0$.*

□

Lemma 8. *The state transition function $\Phi(t, s)$ of following dynamics,*

$$d\mathbf{m}_t = \begin{bmatrix} 0 & 1 \\ 0 & 0 \end{bmatrix} \mathbf{m}_t dt$$

is,

$$\Phi(t, s) = \begin{bmatrix} 1 & t-s \\ 0 & 1 \end{bmatrix}$$

Proof. One can easily verify that such Φ satisfies $\partial\Phi/\partial t = \begin{bmatrix} 0 & 1 \\ 0 & 0 \end{bmatrix} \Phi$. □

Lemma 9 (Chen & Georgiou (2015)). *The optimal control \mathbf{u}_t^* of following problem,*

$$\begin{aligned} \mathbf{u}_t^* &\in \arg \min_{\mathbf{u}_t \in \mathcal{U}} \mathbb{E} \left[\int_0^T \frac{1}{2} \|\mathbf{u}_t\|^2 \right] dt \\ \text{s.t. } \mathbf{d}\mathbf{m}_t &= \begin{bmatrix} 0 & 1 \\ 0 & 0 \end{bmatrix} \mathbf{m}_t dt + \mathbf{u}_t dt + \mathbf{g} d\mathbf{w}_t \\ \mathbf{m}_0 &= m_0, \quad \mathbf{m}_1 = m_1 \end{aligned}$$

is given by

$$\mathbf{u}_t^* = -\mathbf{g}\mathbf{g}^\top \mathbf{P}_t^{-1} (\mathbf{m}_t - \Phi(t, 1)\mathbf{m}_1)$$

Where \mathbf{P}_t follows Lyapunov equation (eq.12) with boundary condition $\mathbf{P}_1 = \mathbf{0}$. and function $\Phi(t, s)$ is the transition matrix from time-step s to time-step t given uncontrolled dynamics.

Proof. See Chen & Georgiou (2015). □

Proposition 10. *The solution of the stochastic bridge problem of linear momentum system (Chen & Georgiou, 2015) is*

$$\mathbf{a}^*(\mathbf{m}_t, t) = g_t^2 P_{11} \left(\frac{\mathbf{x}_1 - \mathbf{x}_t}{1-t} - \mathbf{v}_t \right) \quad \text{where : } \quad P_{11} = \frac{-4}{g_t^2(t-1)}. \quad (14)$$

Proof. From Lemma.9, one can get the optimal control for this problem is

$$\mathbf{u}_t^* = -\mathbf{g}\mathbf{g}^\top \mathbf{P}_t^{-1} (\mathbf{m}_t - \Phi(t, 1)\mathbf{m}_1)$$

where state transition function Φ can be obtained from Lemma.8 and \mathbf{P}_t is the solution of Lyapunov equation and \mathbf{P}_t^{-1} can be found in Lemma.6.

Then we have:

$$\begin{aligned} \mathbf{u}_t^* &= -\mathbf{g}\mathbf{g}^\top \mathbf{P}_t^{-1} (\mathbf{m}_t - \Phi(t, 1)\mathbf{m}_1) \\ &= -\mathbf{g}\mathbf{g}^\top \mathbf{P}_t^{-1} \mathbf{m}_t + \mathbf{g}\mathbf{g}^\top \mathbf{P}_t^{-1} \Phi(t, 1)\mathbf{m}_1 \\ &= -\begin{bmatrix} 0 & 0 \\ 0 & g^2 \end{bmatrix} \mathbf{P}_t^{-1} \mathbf{m}_t + \mathbf{g}\mathbf{g}^\top \mathbf{P}_t^{-1} \begin{bmatrix} 1 & t-1 \\ 0 & 1 \end{bmatrix} \mathbf{m}_1 \\ &= -g_t^2 \begin{bmatrix} 0 & 0 \\ P_{10} & P_{11} \end{bmatrix} \mathbf{m}_t + \begin{bmatrix} 0 & 0 \\ 0 & g_t^2 \end{bmatrix} \begin{bmatrix} P_{00} & P_{01} \\ P_{10} & P_{11} \end{bmatrix} \begin{bmatrix} 1 & t-1 \\ 0 & 1 \end{bmatrix} \mathbf{m}_1 \\ &= -g_t^2 \begin{bmatrix} 0 & 0 \\ P_{10} & P_{11} \end{bmatrix} \mathbf{m}_t + g_t^2 \begin{bmatrix} 0 & 0 \\ P_{10} & P_{11} \end{bmatrix} \begin{bmatrix} 1 & t-1 \\ 0 & 1 \end{bmatrix} \mathbf{m}_1 \\ &= -g_t^2 \begin{bmatrix} 0 & 0 \\ P_{10} & P_{11} \end{bmatrix} \mathbf{m}_t + g_t^2 \begin{bmatrix} 0 & 0 \\ P_{10} & P_{10}(t-1) + P_{11} \end{bmatrix} \mathbf{m}_1 \\ &= \begin{bmatrix} 0 \\ g_t^2 P_{10}(\mathbf{x}_1 - \mathbf{x}_t) + g_t^2 P_{10}(t-1) \cdot \mathbf{v}_1 + g_t^2 P_{11}(\mathbf{v}_1 - \mathbf{v}_t) \end{bmatrix} \\ \text{Plug in } \mathbf{v}_1 &:= \frac{\mathbf{x}_1 - \mathbf{x}_t}{1-t} \\ &= \begin{bmatrix} 0 \\ g_t^2 P_{11} \left(\frac{\mathbf{x}_1 - \mathbf{x}_t}{1-t} - \mathbf{v}_t \right) \end{bmatrix} \end{aligned}$$

□

C.3 MEAN AND COVARIANCE OF SDE

We follow the recipe of Särkkä & Solin (2019). The mean μ_t and variance Σ_t of the matrix of random variable \mathbf{m}_t obey the following respective ordinary differential equations (ODEs):

$$\begin{aligned} d\mu_t &= \mathbf{F}_t \mu_t dt + \mathbf{D}_t dt \\ d\Sigma_t &= \mathbf{F}_t \Sigma_t dt + [\Sigma_t \mathbf{F}_t]^\top dt + \mathbf{g} \mathbf{g}^\top dt \end{aligned}$$

One can solve it by numerically simulating two ODEs whose dimension is just two. Or one can use software such as Inc. (2022) to get analytic solutions.

C.4 DERIVATION FROM SDE TO ODE FOR PHASE DYNAMICS

One can represent the dynamics in the form of,

$$\begin{bmatrix} d\mathbf{x}_t \\ d\mathbf{v}_t \end{bmatrix} = \begin{bmatrix} \mathbf{v}_t \\ \mathbf{F}_t \end{bmatrix} dt + \begin{bmatrix} \mathbf{0} & \mathbf{0} \\ \mathbf{0} & g_t \end{bmatrix} d\mathbf{w}_t \quad \text{s.t. } \mathbf{m}_0 := \begin{bmatrix} \mathbf{x}_0 \\ \mathbf{v}_0 \end{bmatrix} \sim \mathcal{N}(\mu_0, \Sigma_0) \quad (15)$$

as

$$d\mathbf{m}_t = f(\mathbf{m}_t)dt + \mathbf{g}_t d\mathbf{w}_t$$

And its corresponding Fokker-Planck Partial Differential Equation Øksendal (2003) reads,

$$\frac{\partial p_t}{\partial t} = - \sum_d \frac{\partial}{\partial \mathbf{m}_i} [f_i(\mathbf{m}_t, t)p_t(\mathbf{m}_t)] + \frac{1}{2} \sum_d \frac{\partial^2}{\partial \mathbf{m}_i \partial \mathbf{m}_j} \left[\sum_d \mathbf{g}_t \mathbf{g}_t^\top p_t(\mathbf{m}_t) \right] \quad (16)$$

According to eq.(37) in Song et al. (2020b), One can rewrite such PDE,

$$\frac{\partial p_t}{\partial t} = - \sum_d \frac{\partial}{\partial \mathbf{m}_i} \left\{ f_i(\mathbf{m}_t, t)p_t(\mathbf{m}_t) - \frac{1}{2} [\nabla_{\mathbf{m}} \cdot (\mathbf{g}_t \mathbf{g}_t^\top) + \mathbf{g}_t \mathbf{g}_t^\top \nabla_{\mathbf{m}} \log p(\mathbf{m}_t)] \right\} \quad (17)$$

$$\text{due to the fact } \mathbf{g}_t \equiv \begin{bmatrix} \mathbf{0} & \mathbf{0} \\ \mathbf{0} & g_t \end{bmatrix} \quad (18)$$

$$= - \sum_d \frac{\partial}{\partial \mathbf{m}_i} \left\{ f_i(\mathbf{m}_t, t)p_t(\mathbf{m}_t) - \frac{1}{2} [g_t^2 \nabla_{\mathbf{v}} \log p(\mathbf{m}_t)] \right\} \quad (19)$$

Then one can get the equivalent ODE:

$$d\mathbf{m}_t = \left[f(\mathbf{m}_t, t) - \frac{1}{2} g_t^2 \nabla_{\mathbf{v}} \log p(\mathbf{m}_t) \right] dt + \mathbf{g}_t d\mathbf{w}_t \quad (20)$$

C.5 DECOMPOSITION OF COVARIANCE MATRIX AND REPRESENTATION OF SCORE

Here we follow the procedure in Dockhorn et al. (2021). Given the covariance matrix Σ_t , the decomposition of the positive definite symmetric matrix is,

$$\Sigma_t = \mathbf{L}_t^\top \mathbf{L}_t \quad (21)$$

Where,

$$\mathbf{L}_t = \begin{bmatrix} L_t^{xx} & L_t^{xv} \\ L_t^{xv} & L_t^{vv} \end{bmatrix} = \begin{bmatrix} \sqrt{\Sigma_t^{xx}} & 0 \\ \frac{\Sigma_t^{xv}}{\sqrt{\Sigma_t^{xx}}} & \sqrt{\frac{\Sigma_t^{xx} \Sigma_t^{vv} - \Sigma_t^{xv} \Sigma_t^{vx}}{\Sigma_t^{xx}}} \end{bmatrix} \quad (22)$$

We borrow results from Dockhorn et al. (2021), the score function reads,

$$\begin{aligned} \nabla_{\mathbf{m}} \log p(\mathbf{m}_t | \mathbf{m}_1) &= -\nabla_{\mathbf{m}_t} \frac{1}{2} (\mathbf{m}_t - \mu_t) \Sigma_t^{-1} (\mathbf{m}_t - \mu_t) \\ &= -\Sigma_t^{-1} (\mathbf{m}_t - \mu_t) \\ &\text{Cholesky decomposition of } \Sigma_t \\ &= -\mathbf{L}^{-T} \mathbf{L}^{-1} (\mathbf{m}_t - \mu_t) \\ &= -\mathbf{L}^{-T} \epsilon \end{aligned}$$

The form of \mathbf{L} reads,

$$\mathbf{L}_t = \begin{bmatrix} \sqrt{\Sigma_t^{xx}} & 0 \\ \frac{\Sigma_t^{xv}}{\sqrt{\Sigma_t^{xx}}} & \sqrt{\frac{\Sigma_t^{xx}\Sigma_t^{vv} - (\Sigma_t^{xv})^2}{\Sigma_t^{xx}}} \end{bmatrix}$$

and the transpose inverse of \mathbf{L} reads,

$$\mathbf{L}_t^{-T} = \begin{bmatrix} \frac{1}{\sqrt{(\Sigma_t^{xx} + \epsilon_{xx})}} & \frac{-\Sigma_t^{xv}}{\sqrt{(\Sigma_t^{xx})(\Sigma_t^{vv}) - (\Sigma_t^{xv})^2}} \\ 0 & \frac{\sqrt{\Sigma_t^{xx}}}{\sqrt{(\Sigma_t^{xx})(\Sigma_t^{vv}) - (\Sigma_t^{xv})^2}} \end{bmatrix}$$

Hence, the score function reads,

$$\nabla_{\mathbf{v}} \log p(\mathbf{m}_t | \mathbf{m}_1) = - \underbrace{\frac{\sqrt{\Sigma_t^{xx}}}{\sqrt{(\Sigma_t^{xx} + \epsilon_{xx})(\Sigma_t^{vv} + \epsilon_{vv}) - (\Sigma_t^{xv})^2}} \epsilon_1}_{\ell_t}$$

C.6 REPRESENTATION OF ACCELERATION \mathbf{a}_t

As been shown in Proposition.3, the optimal control can be represented as,

$$\begin{aligned} \mathbf{a}_t^* &= g_t^2 P_{11} \left(\frac{\mathbf{x}_1 - \mathbf{x}_t}{1-t} - \mathbf{v}_t \right) \\ &= g_t^2 P_{11} \frac{\mathbf{x}_1}{1-t} - g_t^2 P_{11} \left(\frac{\mathbf{x}_t}{1-t} + \mathbf{v}_t \right) \\ &= g_t^2 P_{11} \frac{\mathbf{x}_1}{1-t} - g_t^2 P_{11} \left(\frac{\mu_t^x + L_t^{xx} \epsilon_0}{1-t} + (\mu_t^v + L_t^{xv} \epsilon_0 + L_t^{vv} \epsilon_1) \right) \\ &= g_t^2 P_{11} \left[\left(\frac{\mathbf{x}_1 - \mu_t^x}{1-t} - \mu_t^v \right) - \left(\frac{L_t^{xx}}{1-t} \epsilon_0 + L_t^{xv} \epsilon_0 + L_t^{vv} \epsilon_1 \right) \right] \end{aligned}$$

solving eq.C.3 we can get : $\mathbf{x}_t = \frac{1}{3} \mathbf{x}_1 t^2 (t^2 - 4t + 6)$, $\mathbf{v}_t = \frac{4t \mathbf{x}_1}{3} (t^2 - 3t + 3)$

Plug in $\mathbf{x}_t, \mathbf{v}_t$

$$\begin{aligned} &= g_t^2 P_{11} \left[\left(\frac{\mathbf{x}_1 - \frac{1}{3} \mathbf{x}_1 t^2 (6 - 4t + t^2)}{1-t} - \frac{4t \mathbf{x}_1}{3} (t^2 - 3t + 3) \right) - \left(\frac{L_t^{xx}}{1-t} \epsilon_0 + L_t^{xv} \epsilon_0 + L_t^{vv} \epsilon_1 \right) \right] \\ &= g_t^2 P_{11} \left[\left(\frac{(-t^4 + 4t^3 - 6t^2 + 3)}{3(1-t)} - \frac{4t}{3} (t^2 - 3t + 3) \right) \mathbf{x}_1 - \left(\frac{L_t^{xx}}{1-t} \epsilon_0 + L_t^{xv} \epsilon_0 + L_t^{vv} \epsilon_1 \right) \right] \\ &= g_t^2 P_{11} \left[\left(\frac{-(t-1)(t^3 - 3t^2 + 3t + 3)}{3(1-t)} - \frac{4t}{3} (t^2 - 3t + 3) \right) \mathbf{x}_1 - \left(\frac{L_t^{xx}}{1-t} \epsilon_0 + L_t^{xv} \epsilon_0 + L_t^{vv} \epsilon_1 \right) \right] \\ &= g_t^2 P_{11} \left[\left(\frac{(t^3 - 3t^2 + 3t + 3)}{3} - \frac{1}{3} (4t^3 - 12t^2 + 12t) \right) \mathbf{x}_1 - \left(\frac{L_t^{xx}}{1-t} \epsilon_0 + L_t^{xv} \epsilon_0 + L_t^{vv} \epsilon_1 \right) \right] \\ &= g_t^2 P_{11} \left[(1-t)^3 \mathbf{x}_1 - \left(\frac{L_t^{xx}}{1-t} \epsilon_0 + L_t^{xv} \epsilon_0 + L_t^{vv} \epsilon_1 \right) \right] \\ &= 4(1-t)^2 \mathbf{x}_1 + g_t^2 P_{11} \left(\frac{L_t^{xx}}{1-t} \epsilon_0 + L_t^{xv} \epsilon_0 + L_t^{vv} \epsilon_1 \right) \end{aligned}$$

C.7 REPRESENTATION OF ACCELERATION \mathbf{a}_t

We use

$$\lambda(t) = \frac{1}{1-t}$$

For all experiments. We admit that this might not be an optimal selection.

C.8 NORMALIZER OF AGM-SDE AND AGM-ODE

Since the optimal control term can be represented as,

$$\mathbf{a}^*(\mathbf{m}_t, t) = 4\mathbf{x}_1(1-t)^2 - g_t^2 P_{11} \left[\left(\frac{L_t^{xx}}{1-t} + L_t^{xv} \right) \boldsymbol{\epsilon}_0 + L_t^{vv} \boldsymbol{\epsilon}_1 \right].$$

Then we introduce the normalizer as

$$\begin{aligned} \mathbf{z}_{SDE} &= \sqrt{(4(1-t)^2 \cdot \sigma_{data})^2 + g_t^2 P_{11} \left[\left(\frac{L_t^{xx}}{1-t} + L_t^{xv} \right)^2 + (L_t^{vv})^2 \right]} \\ \mathbf{z}_{ODE} &= \sqrt{(4(1-t)^2 \cdot \sigma_{data})^2 + g_t^2 P_{11} + g_t^2 P_{11} \left(\frac{L_t^{xx}}{1-t} + L_t^{xv} \right)^2 + \left[\left(g_t^2 P_{11} L_t^{vv} - \frac{1}{2} g_t^2 \ell_t \right)^2 \right]} \end{aligned}$$

$$\text{Where } \ell := \sqrt{\frac{\Sigma_t^{xx}}{\Sigma_t^{xx} \Sigma_t^{vv} - (\Sigma_t^{xv})^2}}$$

C.9 EXPONENTIAL INTEGRATOR DERIVATION

As suggested by Zhang & Chen (2022), one can write the discretized dynamics as,

$$\begin{aligned} \begin{bmatrix} \mathbf{x}_{t_{i+1}} \\ \mathbf{v}_{t_{i+1}} \end{bmatrix} &= \Phi(t_{i+1}, t_i) \begin{bmatrix} \mathbf{x}_t \\ \mathbf{v}_t \end{bmatrix} + \sum_{j=0}^r C_{i,j} \begin{bmatrix} \mathbf{0} \\ \mathbf{s}_\theta(\mathbf{m}_{t_{i-j}}, t_{i-j}) \end{bmatrix} \\ \text{Where } C_{i,j} &= \int_t^{t+\delta_t} \Phi(t+\delta_t, \tau) \begin{bmatrix} \mathbf{0} & \mathbf{0} \\ \mathbf{0} & \mathbf{z}_\tau \end{bmatrix} \prod_{k \neq j} \left[\frac{\tau - t_{i-k}}{t_{i-j} - t_{i-k}} \right] d\tau, \quad \Phi(t, s) = \begin{bmatrix} 1 & t-s \\ 0 & 1 \end{bmatrix} \end{aligned} \quad (23)$$

After plugging in the transition kernel $\Phi(t, s)$, one can easily obtain the results shown in (10).

C.10 PROOF OF PROPOSITION.5

The estimated data point \mathbf{x}_1 can be represented as

$$\tilde{\mathbf{x}}_1^{SDE} = \frac{(1-t)(\mathbf{F}_t^\theta + \mathbf{v}_t)}{g_t^2 P_{11}} + \mathbf{x}_t, \text{ or } \tilde{\mathbf{x}}_1^{ODE} = \frac{\mathbf{F}_t^\theta + g_t^2 P_{11}(\alpha_t \mathbf{x}_t + \beta_t \mathbf{v}_t)}{4(t-1)^2 + g_t^2 P_{11}(\alpha_t \mu_t^x + \beta_t \mu_t^v)} \quad (24)$$

for SDE and probabilistic ODE dynamics respectively, and $\beta_t = L_t^{vv} + \frac{1}{2P_{11}}$, $\alpha_t = \frac{(\frac{L_t^{xx}}{1-t} + L_t^{xv}) - \beta_t L_t^{xv}}{L_t^{xx}}$.

Proof. It is easy to derive the representation of \mathbf{x}_1 of the SDE due to the fact that the network is essentially estimating:

$$\begin{aligned} \mathbf{F}_t^\theta &\approx g_t^2 P_{11} \left(\frac{\mathbf{x}_1 - \mathbf{x}_t}{1-t} - \mathbf{v}_t \right) \\ \Leftrightarrow \mathbf{x}_1 &\approx \frac{(1-t)(\mathbf{F}_t^\theta + \mathbf{v}_t)}{g_t^2 P_{11}} + \mathbf{x}_t \end{aligned}$$

It will become slightly more complicated for probabilistic ODE cases. We notice that

$$\begin{aligned} \mathbf{m}_t &= \boldsymbol{\mu}_t + \mathbf{L}\boldsymbol{\epsilon} \\ \Leftrightarrow \mathbf{x}_t &= \boldsymbol{\mu}_t^x + L_t^{xx} \boldsymbol{\epsilon}_1, \quad \mathbf{v}_t = \boldsymbol{\mu}_t^v + L_t^{xv} \boldsymbol{\epsilon}_0 + L_t^{vv} \boldsymbol{\epsilon}_1 \end{aligned}$$

In probabilistic ODE case, the force term can be represented as,

$$\mathbf{F}(\mathbf{m}_t, t) = 4\mathbf{x}_1(1-t)^2 - g_t^2 P_{11} \left[\left(\frac{L_t^{xx}}{1-t} + L_t^{xv} \right) \boldsymbol{\epsilon}_0 + L_t^{vv} \boldsymbol{\epsilon}_1 \right] - \frac{1}{2} g_t^2 \ell \boldsymbol{\epsilon}_1$$

In order to use linear combination of \mathbf{x}_t and \mathbf{v}_t to represent \mathbf{F} one needs to match the stochastic term in \mathbf{F}_t by using

$$\begin{aligned}\alpha_t L_t^{xx} + \beta_t L_t^{xv} &= \underbrace{\frac{L_t^{xx}}{1-t} + L_t^{xv}}_{A_t}, \\ \beta_t L_t^{vv} &= L_t^{vv} + \underbrace{\frac{1}{2P_{11}}}_{B_t}.\end{aligned}$$

The solution can be obtained by:

$$\begin{aligned}\beta_t &= \frac{B_t}{L_t^{vv}} \\ \alpha_t &= \frac{A_t - \beta_t L_t^{xv}}{L_t^{xx}}\end{aligned}$$

□

By substitute it back to \mathbf{F}_t , one can get:

$$\begin{aligned}\mathbf{F}(\mathbf{m}_t, t) &= 4\mathbf{x}_1(1-t)^2 - g_t^2 P_{11} [\alpha_t(\mathbf{x}_t - \mu_t^x) + \beta_t(\mathbf{v}_t - \mu_t^v)] \\ &= [4(1-t)^2 + g_t^2 P_{11}(\alpha_t \mu_t^x + \beta_t \mu_t^v)] \mathbf{x}_1 - g_t^2 P_{11} [\alpha_t \mathbf{x}_t + \beta_t \mathbf{v}_t] \\ \Leftrightarrow \mathbf{x}_1 &= \frac{\mathbf{F}_t^\theta + g_t^2 P_{11}(\alpha_t \mathbf{x}_t + \beta_t \mathbf{v}_t)}{4(t-1)^2 + g_t^2 P_{11}(\alpha_t \mu_t^x + \beta_t \mu_t^v)}\end{aligned}$$

D EXPERIMENTAL DETAILS

Training: We stick with hyperparameters introduced in the section 4. We use AdamW (Loshchilov & Hutter, 2017) as our optimizer and Exponential Moving Averaging with the exponential decay rate of 0.9999. We use $8 \times$ Nvidia A100 GPU for all experiments. For further, training setup, please refer to Table 6.

Table 6: Additional experimental details

dataset	Training Iter	Learning rate	Batch Size	network architecture
toy	0.05M	1e-3	1024	ResNet(Dockhorn et al., 2021)
CIFAR-10	0.5M	1e-3	512	NCSN++(Karras et al., 2022)
AFHQv2	0.5M	1e-3	512	NCSN++(Karras et al., 2022)
ImageNet-64	0.8M	2e-4	512	ADM(Dhariwal & Nichol, 2021)

Sampling: For Exponential Integrator, we choose the multistep order $w = 2$ consistently for all experiments. Different from previous work (Dockhorn et al., 2021; Karras et al., 2022; Zhang et al., 2023), we use quadratic timesteps scheme with $\kappa = 2$:

$$t_i = \left(\frac{N-i}{N} t_0^{\frac{1}{\kappa}} + \frac{i}{N} t_N^{\frac{1}{\kappa}} \right)^\kappa$$

Which is opposite to the classical DM. Namely, the time discretization will get larger when the dynamics is propagated close to data. For numerical stability, we use $t_0 = 1E-5$ for all experiments. For $NFE = 5$, we use $t_N = 0.5$ and $NFE = 10$, $T_N = 0.7$. For the rest of the sampling, we use $t_N = 0.999$.

Due to the fact that EDM(Karras et al., 2022) is using second-order ODE solver, in practice, we allow it to have an extra one NFE as reported for all the tables.

E ADDITIONAL FIGURES

We demonstrate the samples for different datasets with varying NFE.

E.1 CIFAR-10

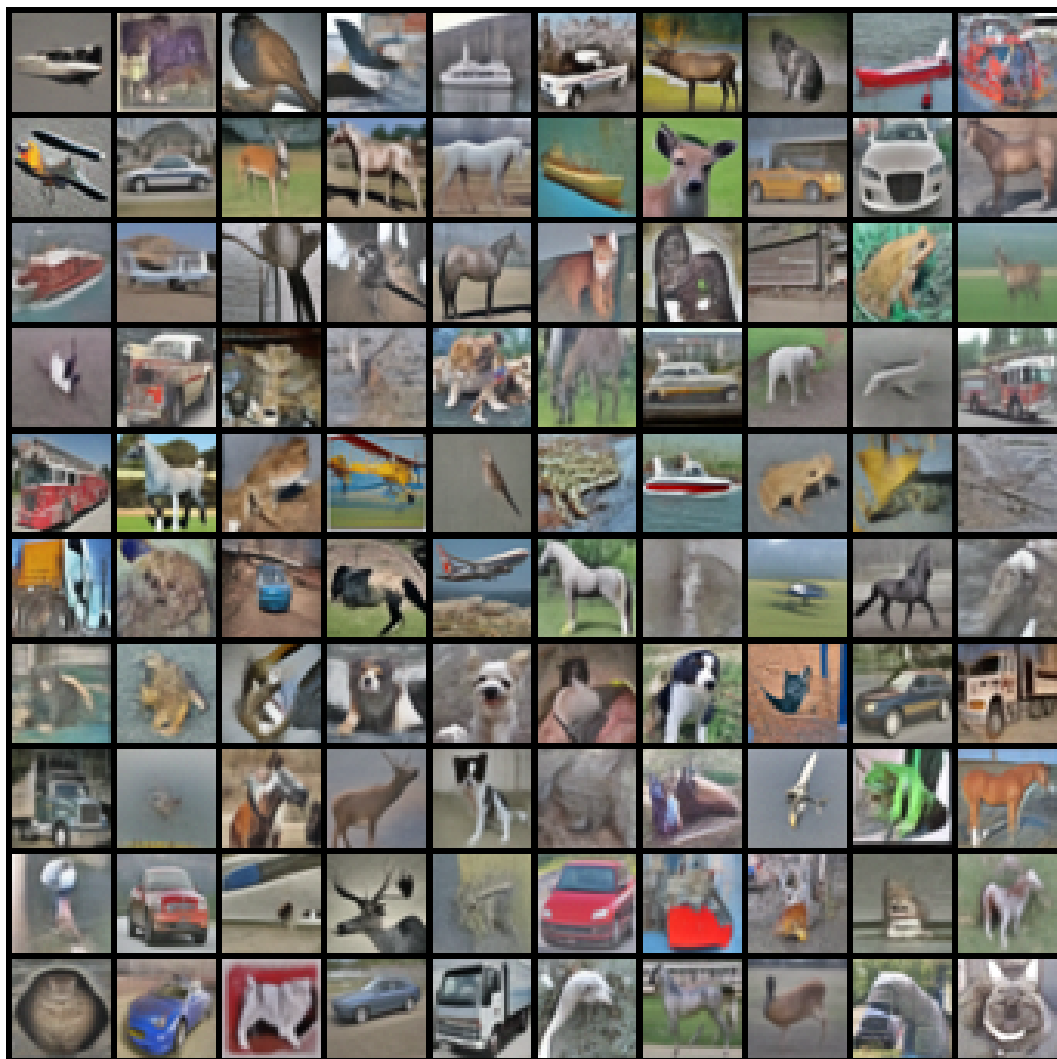


Figure 7: AGM-ODE Uncurated CIFAR-10 samples with NFE=5

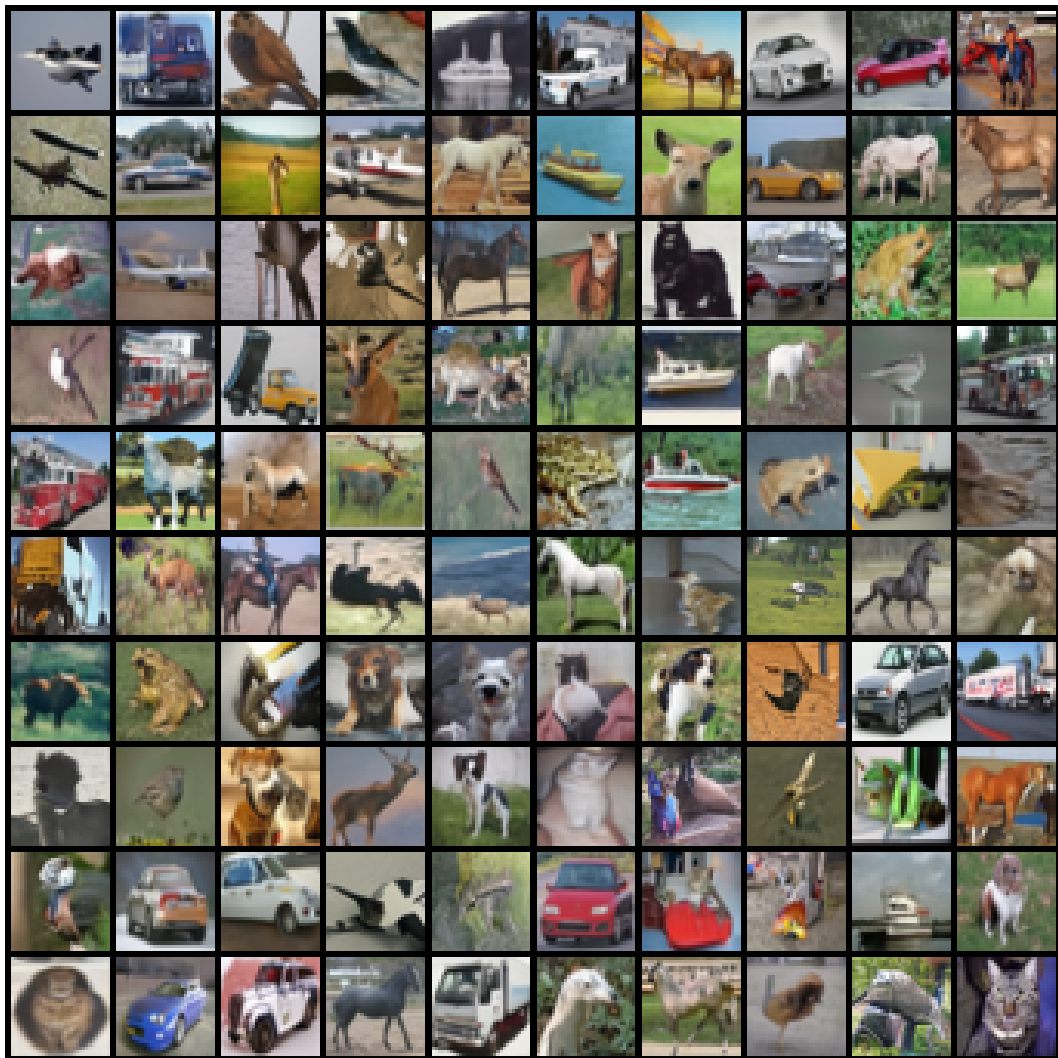


Figure 8: AGM-ODE Uncurated CIFAR-10 samples with NFE=10

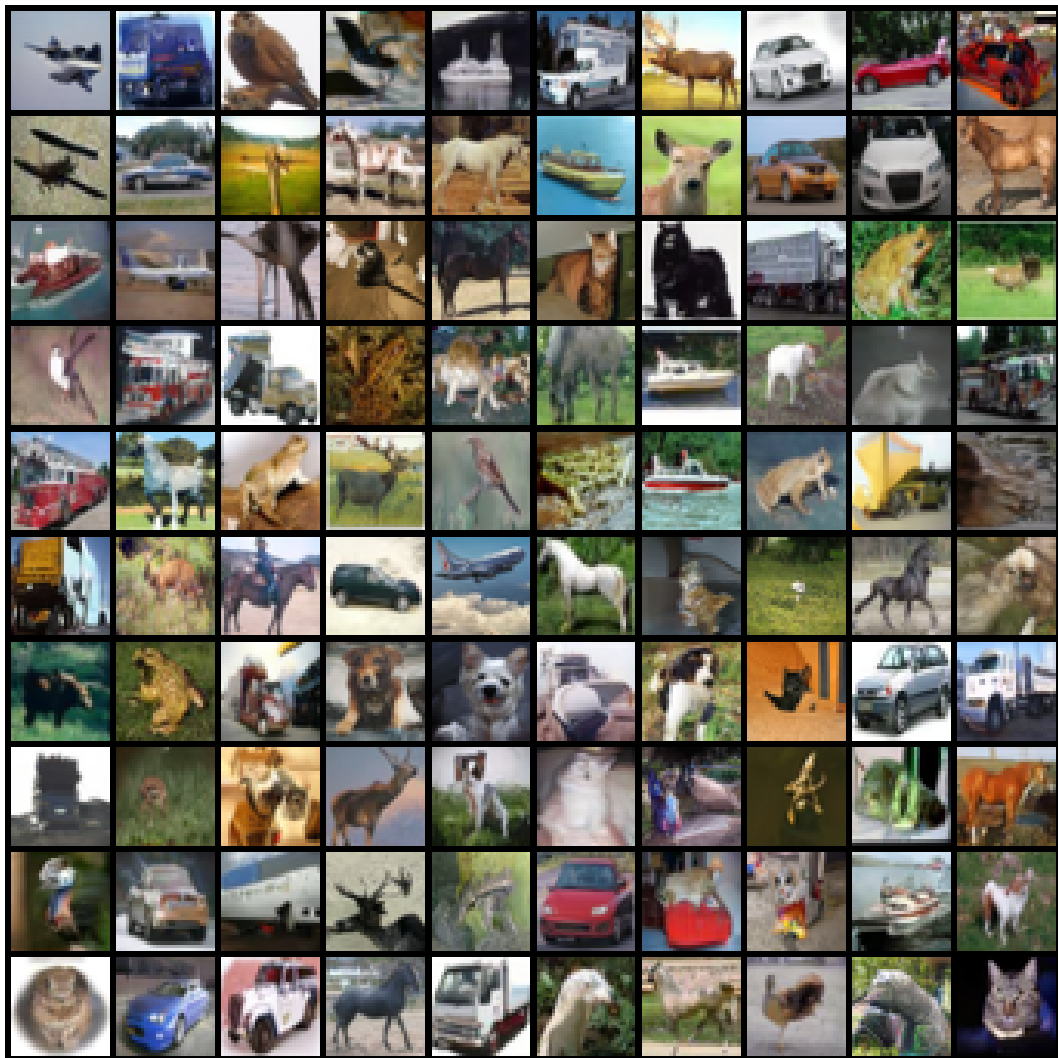


Figure 9: AGM-ODE Uncurated CIFAR-10 samples with NFE=20

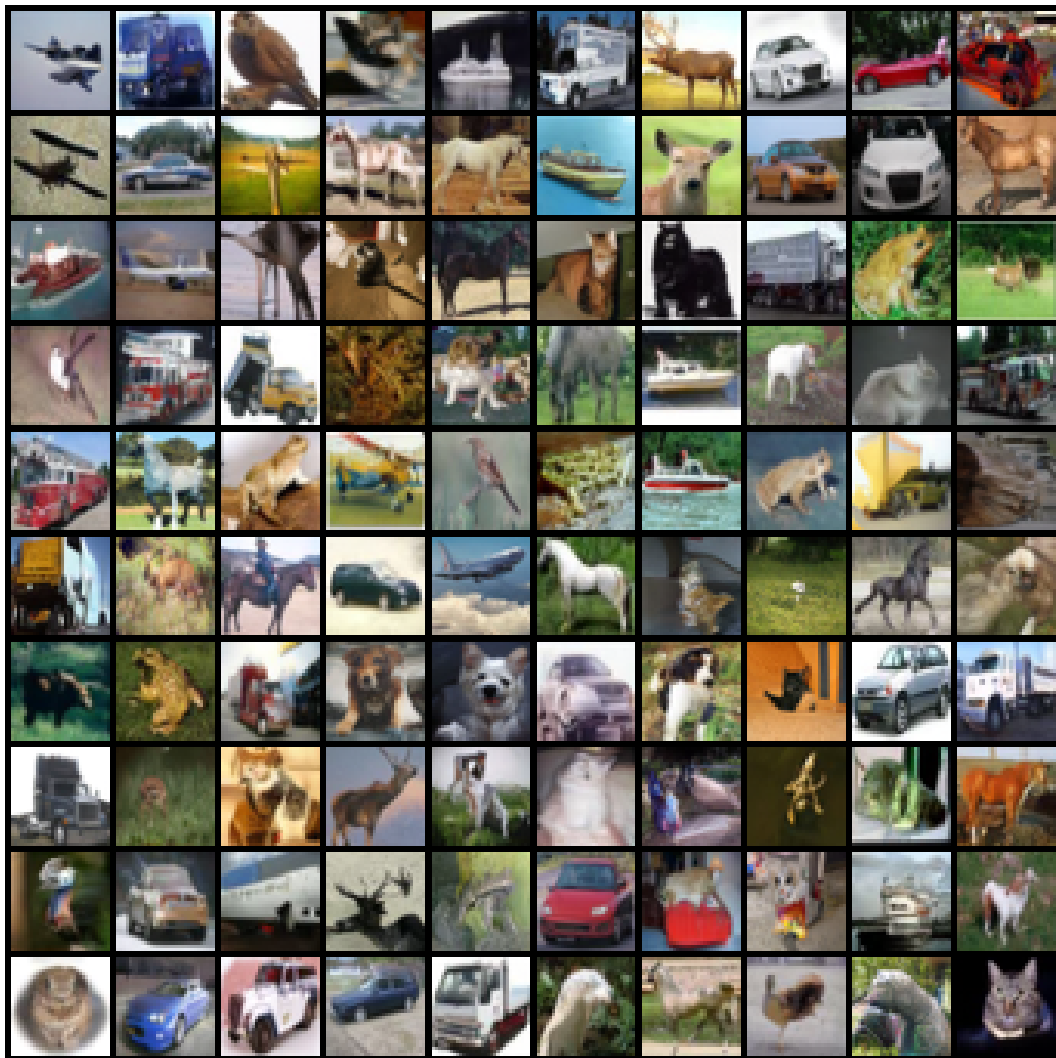


Figure 10: AGM-ODE Uncurated CIFAR-10 samples with NFE=50

E.2 AFHQv2

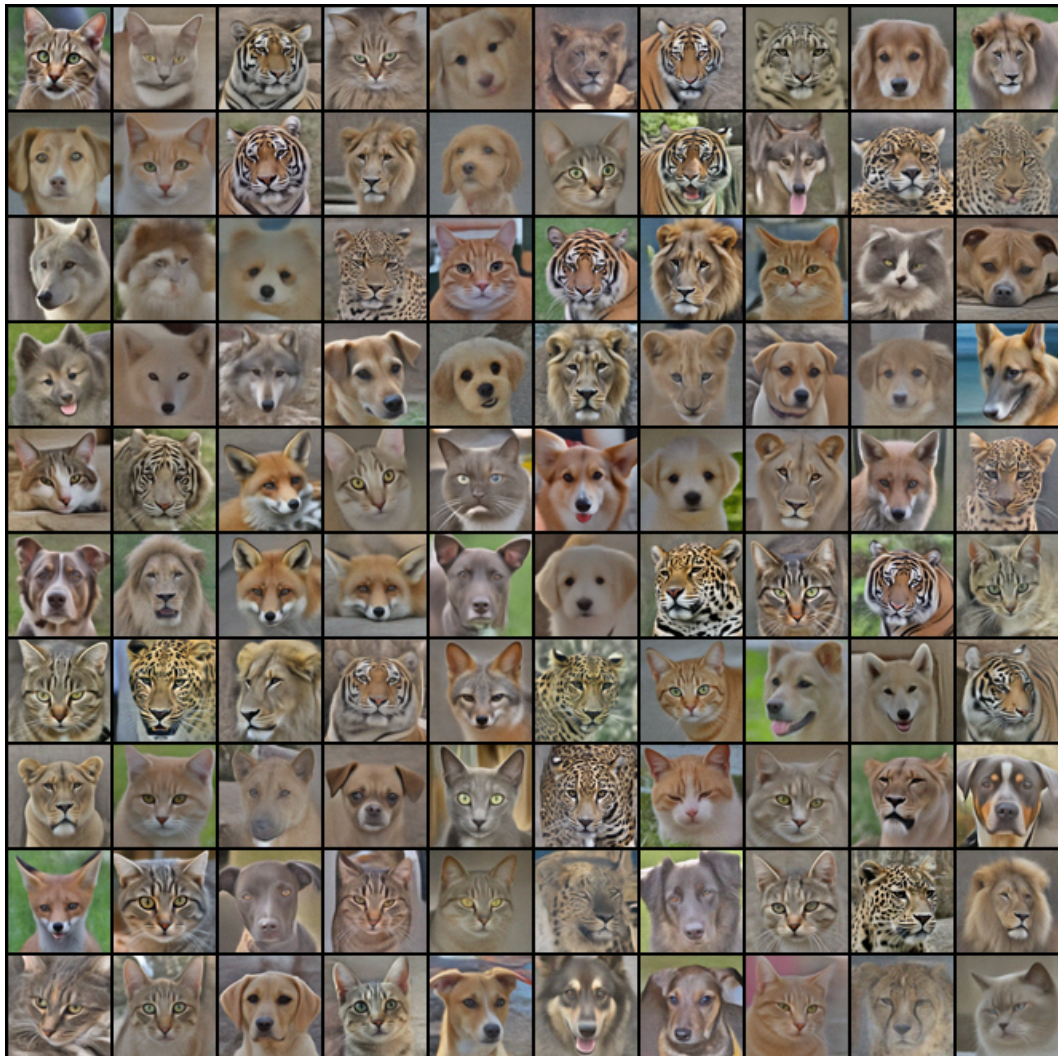


Figure 11: AGM-ODE Uncurated CIFAR-10 samples with NFE=5



Figure 12: AGM-ODE Uncurated CIFAR-10 samples with NFE=10



Figure 13: AGM-ODE Uncurated CIFAR-10 samples with NFE=20

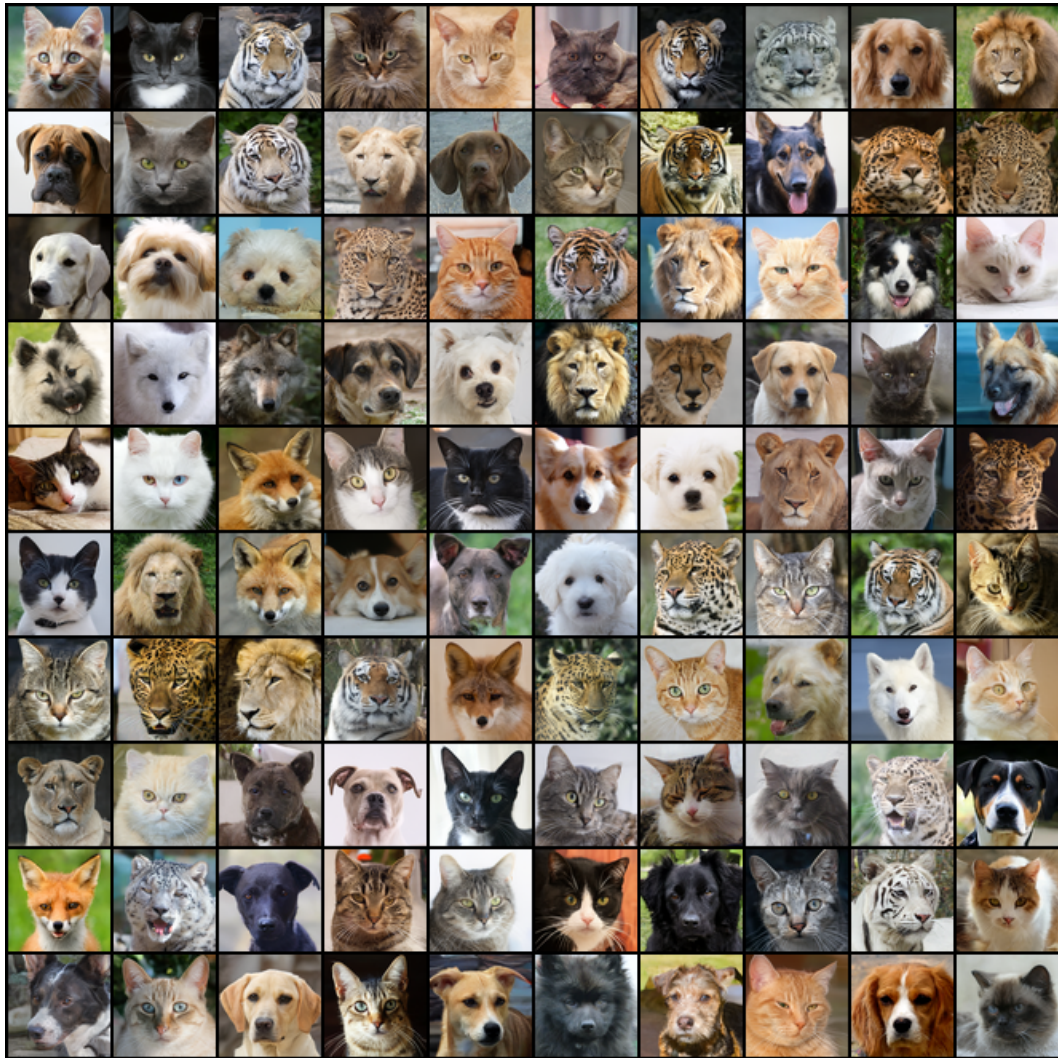


Figure 14: AGM-ODE Uncurated CIFAR-10 samples with NFE=50

E.3 IMAGENET-64



Figure 15: AGM-ODE Uncurated CIFAR-10 samples with NFE=10

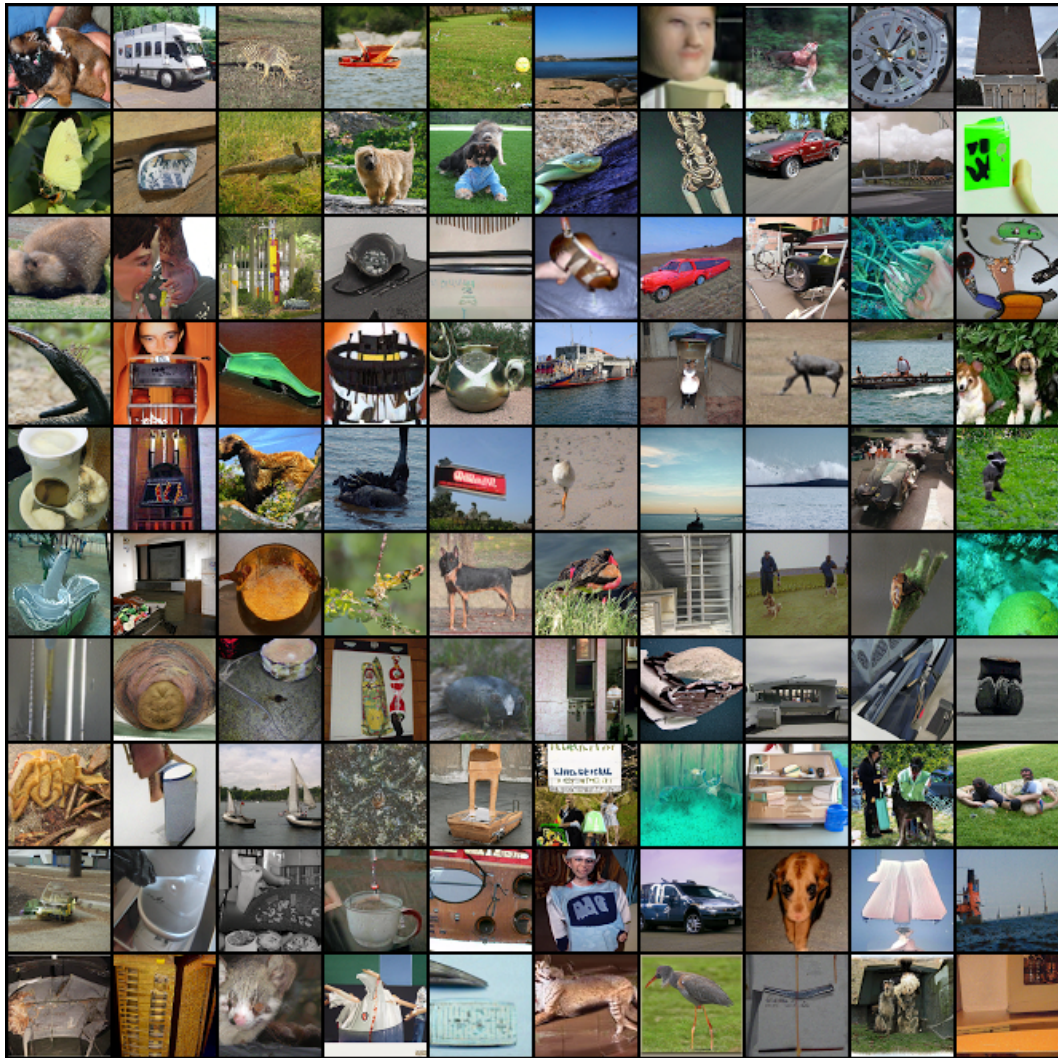


Figure 16: AGM-ODE Uncurated CIFAR-10 samples with NFE=20

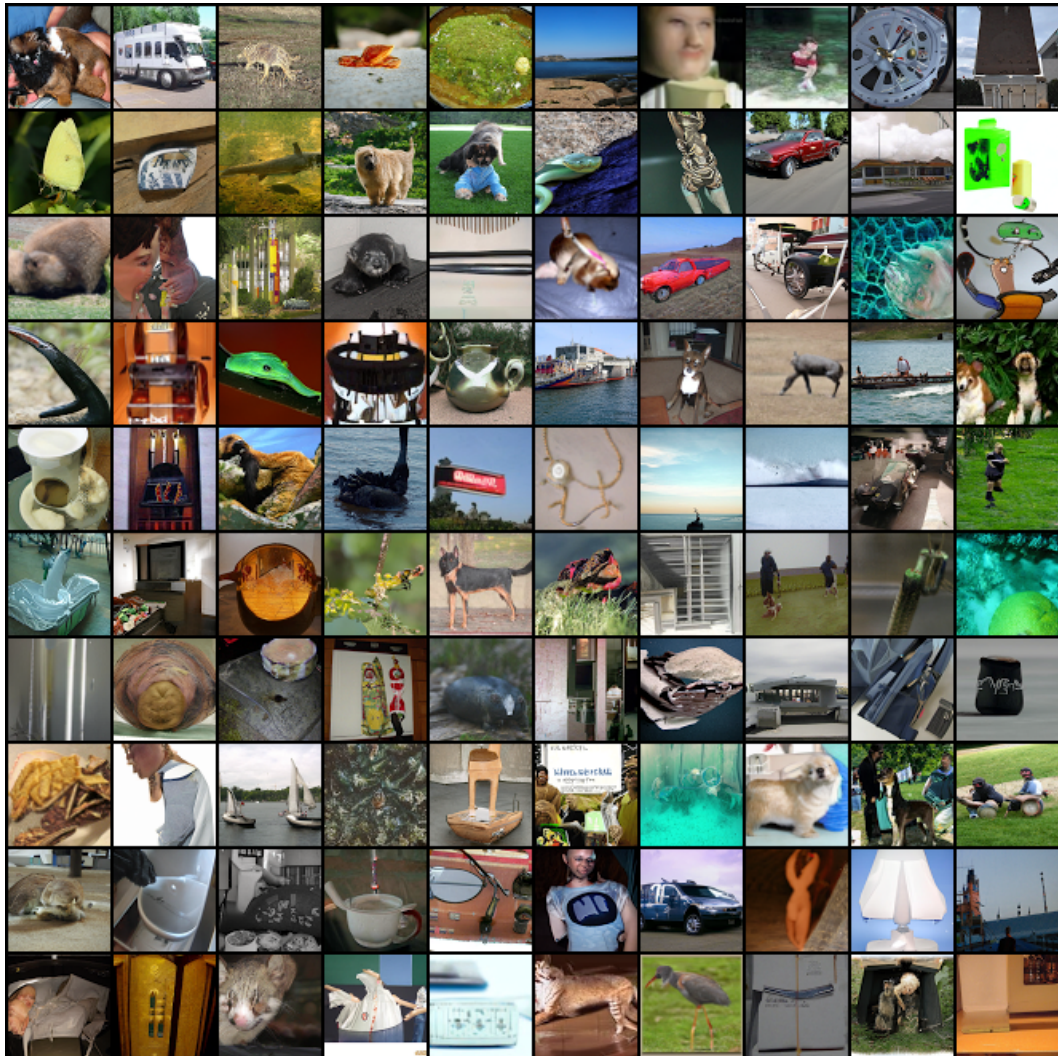


Figure 17: AGM-ODE Uncurated CIFAR-10 samples with NFE=50